

Cover page

Exam information

NFYK15800E - Climate Change Thesis 30 ECTS, Niels Bohr Institute - Kontrakt:105470 (Michelle Shu-Ting Lee)

Handed in by

Michelle Shu-Ting Lee
nxv997@alumni.ku.dk

Exam administrators

Eksamensteam, SCIENCE Uddannelse
eksamen@science.ku.dk

Assessors

Helle Astrid Kjær
Examiner
hellek@nbi.ku.dk
☎ +4535320629

Paul Travis Vallelonga
Examiner
ptravis@nbi.ku.dk
☎ +4535320043

Nanna Bjørnholt Karlsson
Co-examiner
nbk@geus.ku.dk

Hand-in information

Titel: Climate proxies based on the NEEM ice core for the Holocene period 4000-7000 years B2K: An integrated CFA and IEC method for the NEEM brittle zone



Climate proxies based on the NEEM ice core for the Holocene period 4000-7000 years B2K

An integrated CFA and IEC method for the NEEM brittle zone



MSc Climate Change Thesis

Michelle Shu-Ting Lee

Physics of Ice, Earth and Climate (PICE), formerly the
Centre for Ice and Climate (CIC)

Niels Bohr Institute
University of Copenhagen

Supervisors: Helle Astrid Kjær and Paul Travis Vallelonga

Submitted on: 31 May 2019

Name of department: Physics of Ice, Climate and Earth (PICE), Niels Bohr Institute

Author(s): Michelle Shu-Ting Lee

Title and subtitle: Climate proxies based on the NEEM ice core for the Holocene period 4000-7000 years B2K: An integrated CFA and IEC method for the NEEM brittle zone

Topic description: The NEEM ice core consists of a brittle zone that correlates to part of the Holocene, between 4,000 to 7,000 years B2K. This brittle zone potentially holds valuable information regarding past climate during the Holocene, despite its susceptibility to damage during analysis. By using continuous flow analysis and ion exchange chromatography techniques, this project investigates the brittle zone through various ionic species that serve as proxies for parameters such as wind speed, sea ice, and volcanic activity that together give reasoned proxies of climate at the time. In this project, NEEM ice core samples of this period are sorted, decontaminated, prepped, and then tested. The output from ion chromatograph is translated to ultimately show concentrations of various ionic species. The results are compared with published datasets for validation and small-scale analysis is conducted.

Supervisor: Helle Astrid Kjær and Paul Vallelonga

Submitted on: 31 May 2019

Grade: [X]

Number of study units:

2 3

Number of characters: [XXX]

[Lorem ipsum in eternum]

[Lorem ipsum in eternum]

Abstract

The NEEM ice core consists of a brittle zone (BZ) that correlates to part of the Holocene, between 4,000 to 7,000 years before present. This brittle zone potentially holds valuable information regarding climate during the Holocene, despite its susceptibility to damage during analysis. By using integrated CFA and ion exchange chromatography techniques (IEC), this project investigates the brittle zone through various ionic species that serve as proxies for parameters such as wind speed, sea ice, and volcanic activity that together provide reasoned proxies and analysis of climate at the time. In this project, NEEM ice core samples of this period are sorted, decontaminated, prepped, and then tested. The output from ion chromatograph is translated to ultimately show concentrations of various ionic species. These results are compared with published datasets for several ions to provide verification and indication of true values. Specific areas of interests are further analyzed in greater detail to identify potential climate events or areas of higher seasonal intensity. No data has been available for the NEEM BZ until now and this study begins to unravel the NEEM BZ and Holocene.

Danish

NEEM-iskernen indeholder en zone af skrøbelig is som dækker en del af tidsperioden Holocæn, fra ca. 4.000-7.000 år f.v.t. Zonen med skrøbelig is kan potentielt set indeholde brugbar information om klimaet under Holocæn, på trods af dens modtagelighed overfor skader under målinger. Ved brug af integrerede CFA- og ionkromatografiske teknikker undersøger dette projekt zonen med skrøbelig is ved analyse af forskellige ionarter, der fungerer som proxyer for parametre såsom vindhastighed, hav is, og vulkansk aktivitet, og disse proxyer kan bidrage til at tegne et billede af tidsperiodens klimaudsving. I dette projekt vil prøver fra NEEM-iskernen blive sorteret, dekontamineret, klargjort, og dernæst undersøgt. Resultaterne fra ionkromatografien vil dernæst blive konverteret til endeligt at kunne vise koncentrationer af diverse ionarter. For at kunne verificere, og give en indikation af realistiske og brugbare værdier, vil resultaterne blive sammenlignet med allerede publicerede datasæt for diverse ioner. Områder af specifik interesse vil blive yderligere analyseret for at kunne identificere potentielle klimaudsving, eller områder med mere intense årstidsvariationer. Der har hidtil ikke været data tilgængeligt for zonen med skrøbelig is i NEEM-iskernen, og dette studie sætter dermed gang i undersøgelsen af zonen med skrøbelig is, og Holocæn, i NEEM-iskernen.

Translated by Mathias Skov Jensen

Acknowledgements

Upon the completion of this project, I have had an opportunity to reflect on the wonderful experience and would like to thank and acknowledge a few groups and individuals. Firstly, I have massive gratitude towards my supervisors Paul Vallelonga and Helle Astrid Kjær. They have been immensely supportive, always with their door (or email) open for questions and to help. I could not have figured out the necessary code nor have created what I think is a fruitful discussion without them. They are great educators and I have been inspired and learned so much from them. I would also like to express my gratitude towards Anders Svensson for allowing me to enter his office unexpectedly to ask questions and providing helpful insight on the spot.

Of course this is not possible without the existence of Physics of Ice, Climate and Earth (PICE), formerly known as the Centre for Ice and Climate (CIC). They have created a supportive, innovative and educational scientific community with several coffee machines, fresh fruit on a bi-weekly basis and Friday lunch. Furthermore, I would also like to thank the Bern EastGrip CFA team for having me there earlier this year to learn so much about CFA and ice core chemistry in such a short time.

Thank you to friends Estelle, Mathias and Mirjam on the ground floor “Istunnelen” for jokes in between writing and for help with data, code and translations. Your advice is always valued and appreciated as is your friendship outside of PICE. I also thank my family for their continued support of my endeavors in Copenhagen. Finally, there are a few other (unequivocally) special people who have played a role in helping me to get where I am, but I must stop my words here. Just know that you are in my heart.

Table of Contents

<i>Abstract</i>	3
<i>Acknowledgements</i>	4
<i>List of Figures</i>	7
<i>List of Tables</i>	8
1. Introduction	9
1.1 NEEM ice core.....	10
2. Glaciochemistry and Climate	11
2.1 Impurities in Ice	11
2.2 Continuous Flow Analysis (CFA)	15
2.3 Ion Chromatography (IC).....	16
3. The Brittle Zone (BZ)	18
3.1 Brittle ice	18
3.2 Drill liquid	20
4. Integration of CFA and IC methods for chemistry	20
4.1 Sampling of NEEM BZ.....	20
4.2 CFA for NEEM BZ.....	21
4.3 Ion Chromatography (IC) of BZ.....	22
4.4 CFA and IC data processing	23
5. Results	25
5.1 IC chemistry results with depth and time	25
5.2 IC chemistry results split by time (years B2K)	32
5.3 Comparison of NH_4^+ , NO_3^- , Na^+ and Ca^{2+} values.....	41
5.4 Comparison of SO_4^{2-} values	43
5.5 Comparison of Br^- values	44
5.6 Comparison of NH_4^+ values with GISP2.....	45

5.7 Climate proxies at several depths	47
6. Discussion	54
6.1 IC results with depth and time	54
6.2 Comparison with Schüpbach et al. (2018) for NH_4^+ , NO_3^- , Ca^{2+} and Mg^{2+}	58
6.3 Comparison with Schüpbach et al. (2018) for SO_4^{2-}	59
6.4 Comparison with Spolaor et al. (2016) for bromine	59
6.5 Comparison with GISP2 for NH_4^+	60
6.6 Special Cases for Analysis.....	61
6.7 Conductivity, dust and drill liquid contamination.....	66
6.8 Limitations and Uncertainties	67
7. Conclusion.....	69
References.....	70
Appendix	73

List of Figures

1. Map of Greenland ice core drilling sites
2. Linescan image of an ice core
3. C CFA (Copenhagen CFA) general setup
4. Example of anion chromatogram output using ion exchange chromatography technique
5. Example of fluoride anion calibration curve and function to determine concentration
6. Image of a section of brittle ice
7. Brittle zone transition of air bubbles into air-hydrate crystals
8. Visual of air bubbles transitioning to air-hydrate crystals
9. CFA configuration for this study of NEEM BZ
10. Example of calibration of IC for NEEM BZ
11. Depth vs. cations from IEC results
12. Depth vs. anions from IEC results
13. Time (years B2K) vs. cations from IEC results
14. Time (years B2K) vs. anions from IEC results
15. Cation panel 1 split by time (years B2K)
16. Cation panel 2 split by time (years B2K)
17. Cation panel 3 split by time (years B2K)
18. Cation panel 4 split by time (years B2K)
19. Anions panel 1 split by time (years B2K)
20. Anions panel 2 split by time (years B2K)
21. Anions panel 3 split by time (years B2K)
22. Anions panel 4 split by time (years B2K)
23. Comparison for NH_4^+ , NO_3^- , Na^+ , Ca^{2+} using Schüpbach et al. (2018)
24. Comparison for SO_4^{2-} using Schüpbach et al (2018)
25. Comparison for Br^- values using Spolaor et al. (2016)
26. Comparison for NH_4^+ using GISP2 data
27. Analysis at 810 m (biological activity)
28. Analysis at 885 m (drill liquid contamination)
29. Analysis at 923 m (annual cycle detection)
30. Analysis at 950 m (possibly volcanic)
31. Analysis at 1004 m (possibly volcanic or dust)
32. Analysis of 1009 m (possibly volcanic)

33. Analysis of 1142 m (possibly volcanic)
34. Conductivity and dust sampling demonstrating drill liquid presence
35. Particle size distribution of dust in sample with drill liquid contamination

List of Tables

1. List of impurities in ice and their function as climate proxies
2. Means and standard deviations for IEC results for each cation
3. Means and standard deviations for IEC results for each anion
4. Means and standard deviations for comparison with Schüpbach et al. (2018)
5. Means and standard deviations for SO_4^{2-} comparison with Schüpbach et al. (2018)
6. Means and standard deviations for NH_4^+ comparison with GISP2
7. Sea salt and non-sea salt (nSs) components of various ions that are known to be present in seawater.

1. Introduction

The NEEM (North Greenland Eemian Ice Drilling) drilling between the years of 2007 and 2011 retrieved ice cores dating back to the previous interglacial period known as the Eemian. While chemistry records have been interpreted through various experimental techniques, the NEEM brittle zone (BZ) in between 740 and 1155 m remains an area in which data is missing. The BZ consists of the depths in which air bubbles transform into air-hydrate crystals. Retrieving cores from BZ depths result in fracturing of the ice. The ice fracturing renders the classical CFA technique of measuring chemistry, conductivity and dust unviable. Furthermore, contamination from handling, exposure and drilling liquids complicate the samples for analysis.

In this study, an integration of two techniques to measure chemistry, Continuous Flow Analysis (CFA) and Ion Exchange Chromatography (IEC), is used. The use of CFA is aimed to gather uncontaminated portions of quality selected ice samples into aliquots that will be tested on the ion chromatograph (IC) for anion and cation concentrations. The results are analyzed and compared with data already published for depths at or in close proximity to the BZ. Areas of interest in the BZ are distinguished and a detailed analysis provided.

1.1 NEEM ice core

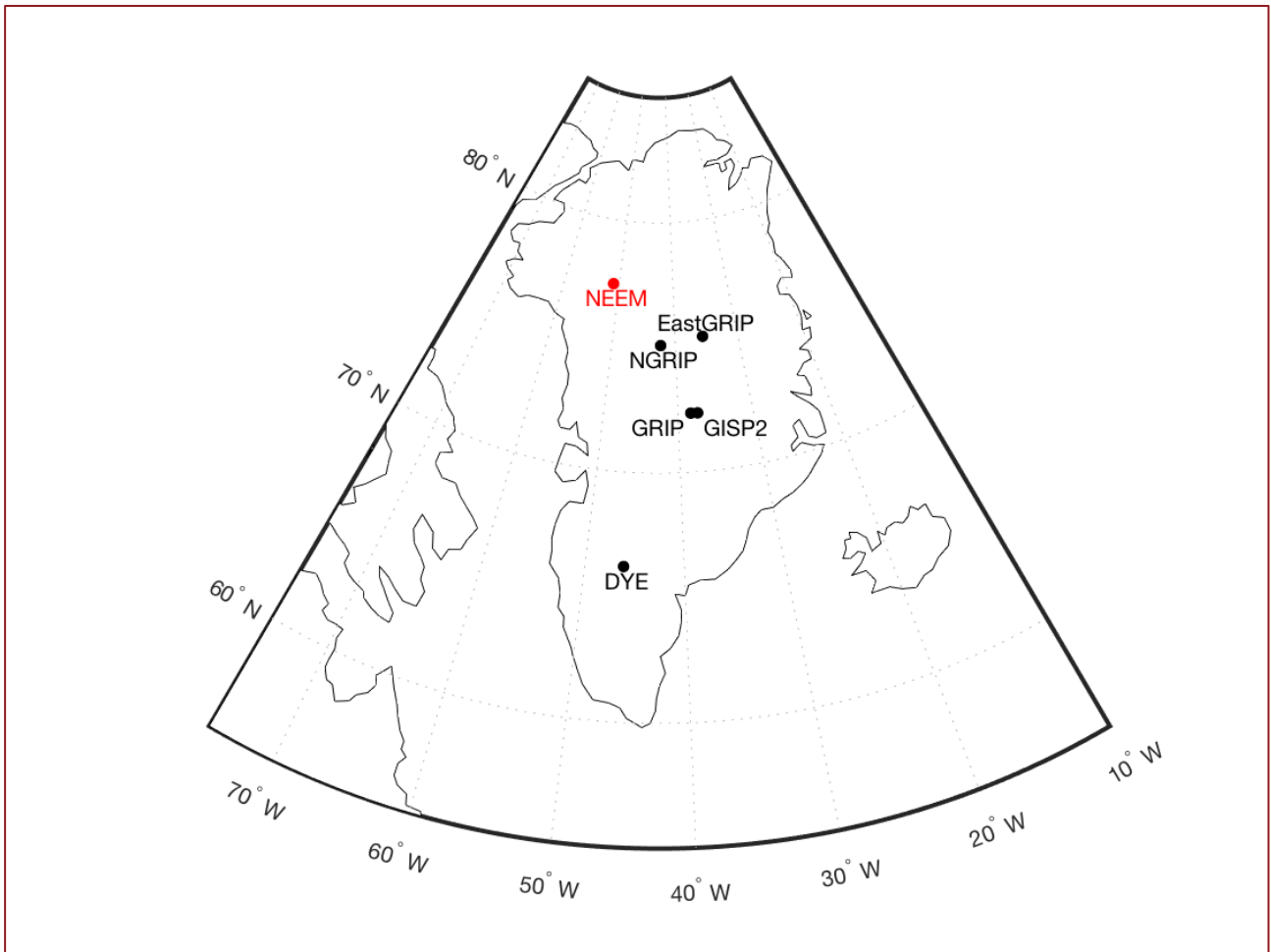


Figure 1 Map of Greenland and ice core drilling sites, including NEEM (courtesy of Helle Astrid Kjær).

The NEEM (North Greenland Eemian Ice Drilling) extends 2540 m to bedrock in NW Greenland (77.45 N, 51.07W) at the elevation of 2479 m with average annual temperature at approximately $-28\text{ }^{\circ}\text{C}$ (Figure 1) (Rasmussen, et al., 2013). The accumulation rate at present day is approximately 0.22 m ice equivalence annually. This is similar to that of GRIP and GISP2, both of which are synchronized chronologically using GICC05 using reference horizons based on matchpoints from DEP (dielectric profiling) and ECM (electrical conductivity measurements). Tephra horizons provided further dating accuracy. The GICC05 was applied to NEEM with thinning functions and an accumulation model up until 122 ka b2k, as that is the farthest that the GICC05 extends. The bottom portion of the core, extending further than 2204.6 m, corresponding to the Eemian period was subject to folding, in which the Antarctic EDML1 timescale based on CH_4 and $\delta^{18}\text{O}$ is applied (Rasmussen, et al., 2013).

An updated version of the NGRIP drill, the Hans Tausen (HT) drill, was used at NEEM (Popp, et al., 2014). It was altered to accommodate the new, more viscous drill liquid known as a combination of Estisol 240 and Coasol. The application of new drill liquid was aimed at faster drill speed, producing ice cores at 3.6 m length at maximum performance. The diameter of NEEM cores were 98 mm with a borehole diameter between 126 and 132 mm (Popp, et al., 2014).

2. Glaciochemistry and Climate

Accumulation in the polar ice caps serve as a unique scope into paleo climate conditions (Legrand & Mayewski, 1997). In areas of particularly low accumulation, precipitation accumulate for millennia. Snow transforms into ice and there remains a continuous record under favorable conditions. At the surface, snow accumulates with densities less than 200 kg m^{-3} . Deeper under the surface, snow transitions to firn with densities ranging between 200 and 800 kg m^{-3} . Finally, ice densities are from 830 kg m^{-3} to 910 kg m^{-3} .

In ice, ancient air is preserved in the remaining trapped air bubbles and can be analyzed for CO_2 and CH_4 trace gases, both of which are proxies of past climate. Furthermore, aerosols and water soluble gases of surrounding ice reveal the composition of impurities that increases understanding of various climatic variables at a given time (Dixon, et al., 2011) (Gabielli, et al., 2005) (Vallelonga, et al., 2004). This field of study, glaciochemistry, uses chemical composition of snow to interpret paleoclimate conditions to understand natural variability and contemporary human influences on natural systems.

2.1 Impurities in Ice

Dust and Wind (Ca^{2+} , Mg^{2+} , K^+ , Li^+)

Impurities in ice cores consist of dust and ionic species. Often, impurities show annual cycles that help to synchronize ice cores and provide a timescale with depth, provided that diffusion and layer thinning do not dissolve the signal (Svensson, 2014). Dust can be observed through stratigraphy and expresses a seasonal cycle, with a dust maximum in spring. The annual layer counting provided by dust allows for sequencing into as far back as the last glacial period (Svensson, 2014). As ionic species, dust levels can be interpreted through Ca^{2+} , Mg^{2+} , K^+ and Li^+

concentrations (Fischer, et al., 2007) (Legrand & Mayewski, 1997) (Siggard-Andersen, et al., 2002). In the Last Glacial Maximum (LGM), mineral dust concentrations in Greenland were at times a factor of 80 greater than the present interglacial. In Greenland, mineral dust derives from Asian deserts and in Antarctica, dust originates from Patagonia. Aridity in the Northern Hemisphere changes between the glacial and interglacial periods in regions such as the Sahara, Middle East, Asia, and the US, changing the sources of dust. In addition to aridity, volcanoes, vegetation cover, organic matter, accumulation rates, and frequency of precipitation all play a role in deposition of dust in Greenland (Svensson, et al., 2000).

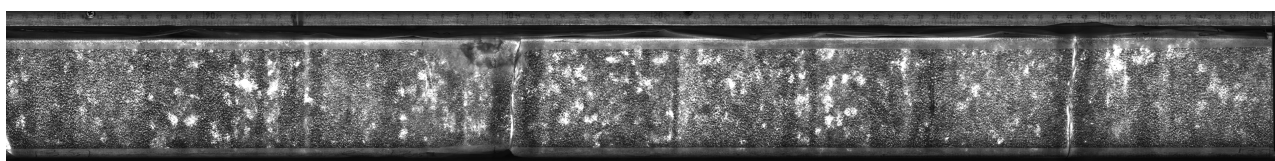


Figure 2 Linescan image showing dust impurities in ice (Bags 1351-1352).

The changes in source and transportation are archived in ice core fluxes of sea salt and mineral dust, both of which are heavily influenced by their source regions (Fischer, et al., 2007). Aridity and vegetation cover and be extrapolated from mineral dust composition. The wet and dry deposition of precipitation and aerosol deposition sequences provide a high, at times seasonal, resolution of dust records (Figure 2). Variations in concentrations of dust can be attributed to an integration of production, transport, and deposition, with sources and lifetime in the atmosphere as main contributors (Fischer, et al., 2007) (Lambert, et al., 2008).

Sea Salt (Na^+ , Cl^- , Mg^{2+})

Sea salt aerosols are produced by the wind dispersion of seawater in both the solid (ice) and liquid state (Fischer, et al., 2007). The dispersion is heavily influenced by three factors: production, transportation and deposition of sea salt and visualized chemically through the presence of Na^+ , Cl^- and Mg^{2+} . Mg^{2+} is also a proxy for dust composition. Uplifting of sea salt particles into the atmosphere makes sea salts prone to long distance transport and deposition, in which then, climate factors constitute a large role in. Because climate conditions heavily influence the distribution of sea salts, Na^+ , Cl^- and Mg^{2+} presence in ice cores can be used to gather information about past climatic activities such as cyclones and wind. During glacial periods, sea salt concentrations have been observed to be double that seen in interglacial periods. Furthermore, winter concentrations of sea salt tend to be higher relative to the seasonal cycle (Fischer, et al., 2007).

Biomass burning (NH_4^+ and NO_3^-)

NH_4^+ and NO_3^- , to a lesser extent, from soils serve as proxies for the presence of wildfires and their frequency and intensity (Fischer, et al., 2015) (Schüpbach, et al., 2018). Wildfires are indicative of the presence of biomass and ecological activity. The background signals of NH_4^+ detected derive from soil bacteria activity, where there are larger peaks in the summer due to vegetation growth. Atmospheric circulation, transport and deposition all constitute a role in the amount of NH_4^+ detected in ice cores. Changes in ice cover impacts the extent of vegetation and therefore, the amount of NH_4^+ . This relationship between ice and vegetation impacts allows the use of NH_4^+ as a proxy for ecosystem activity. At the transition between the last glacial and interglacial period, 3-5 times increase in NH_4^+ values are observed in the NGRIP ice core (Fischer, et al., 2015).

Deposition (NO_3^-)

Past nitrate values serve as a proxy for the concentration of nitrogen in the atmosphere, but these values are influenced by accumulation, temperature and elevation (Röthlisberger, et al., 2002). The top layer of snow is exposed to post depositional losses of nitrate through the evaporation and photolysis of nitric acid (HNO_3). In general, there is a trend of lower NO_3^- values with lower temperature, with higher NO_3^- values in summer snow than winter snow (Legrand & Mayewski, 1997). Accumulation tends to be higher at sites that are warmer, but determining which factor (temperature or accumulation) has greater effect on NO_3^- is difficult. This general NO_3^- trend is complicated by the post-depositional loss as well as solar activity, making the underlying dynamics of NO_3^- in ice cores difficult to discern (Soon, et al., 2014). Where there are low accumulation rates, generalities do not apply to NO_3^- concentrations. Furthermore, there are observations that support the idea that NO_3^- values interact with SO_4^{2-} from volcanic activity through nitric acid diffusion and reaction with sulfuric acid, but the mechanism is not well understood yet (Röthlisberger, et al., 2002) (Lalraj, et al., 2010).

Volcanos (SO_4^{2-} , F^-)

Large volcanic eruptions result in aerosol plumes entering into the stratosphere, where there is climatic forcing as well as long -distance transport of aerosols (Baroni, et al., 2008). Volcanos that reach the stratosphere disturb the energy balance, often resulting in a period of cooling. H_2SO_4 is deposited into ice cores after a volcanic eruptions and increases in acidity (decrease in pH) are often observed. HF constitutes a secondary acid that is present in ice cores after a volcanic eruption. Li^+ , which is part of the earth's crustal material, also can be observed to

increase in the presence of volcanic activity (Siggard-Andersen, et al., 2002). Volcanic activity observed through SO_4^{2-} is also a means to synchronize ice cores through “reference horizons” and to reconstruct volcanic history (Legrand & Mayewski, 1997).

Sea Ice (Br⁻)

The seasonal cycle of bromide shows higher concentrations in the spring (Spolaor, et al., 2016). Bromide serves as a proxy for first-year sea ice (FYSI) with transport of sea ice resulting in declining values. At NEEM, Br⁻ derives from sea ice of the Canadian Arctic. The formation of FYSI increases salinity of the surrounding in brine channels, frost flowers, and blowing snow, all of which are characteristic of FYSI. There are generally higher concentrations of bromide from sea salt on coastal regions and lower values inland due to depletion (Spolaor, et al., 2016).

ECM and DEP

Electrical conductivity measurements (ECM) measure the direct-current of an ice core, which changes with acidity (Wilhelms, et al., 1998) (Taylor, et al., 1993). Two electrodes with a potential of ~1200 V is dragged along the cut surface of the ice, returning measurements based on H⁺ ions. Acidity is influenced by volcanic activity and dust. Seasonal changes are observed as well as unique events. Dielectric profiling (DEP) measures conductance and capacity through alternating current where two electrodes serve as capacitors and the ice is the dielectric (Wilhelms, et al., 1998). DEP measurements are more capable than ECM in detecting salt and ammonium in ice cores in addition to dust and volcanos.

Table 1. List of impurities in ice and their function as climate proxies.

Climate Proxy	Ions
Acidity, volcanos, salt, ammonium	ECM and DEP
Sea Salt and Wind	Na ⁺ , Cl ⁻ , Mg ²⁺
Dust and Wind	Ca ²⁺ , Mg ²⁺ , K ⁺ , Li ⁺
Sea Ice	Br ⁻
Volcano	SO ₄ ²⁻ , ECM and DEP, Li ⁺ , F1 ⁻
Biological activity	NH ₄ ⁺ , NO ₃ ⁻
Deposition, Temperature and Accumulation	NO ₃ ⁻

2.2 Continuous Flow Analysis (CFA)

This method of analysis has the ability to provide high resolution data in deep cores in which layer thinning is prevalent (Bigler, et al., 2011). Continuous flow analysis (CFA) marries many analytical measurements and techniques into one setup and reduces the amount of ice necessary to produce an array of data. In CFA, a continuous liquid stream from the center of the core flows through a debubbler, in which gas measurements can be taken, and through lines that lead into chemistry measurements, dust and conductivity (Bigler, et al., 2011).

In a freezer, the ice core is melted continuously on a gold-plated melthead (Kaufmann, et al., 2008). The ice is placed in a frame of about 33 x 33 mm in which only the uncontaminated center of the cores consisting of meltwater and air goes into sampling lines. Ice is placed into half meter frames that are mounted in the freezer on top of a melthead with nickel and gold, providing effective conduciveness from the electrical cartridge heater. A camera is placed in the freezer near the melthead to monitor progress. LCD screens and controls are adjacent to the setup. Meltrates vary ideally between 3-4 cm/min (Kaufmann, et al., 2008).

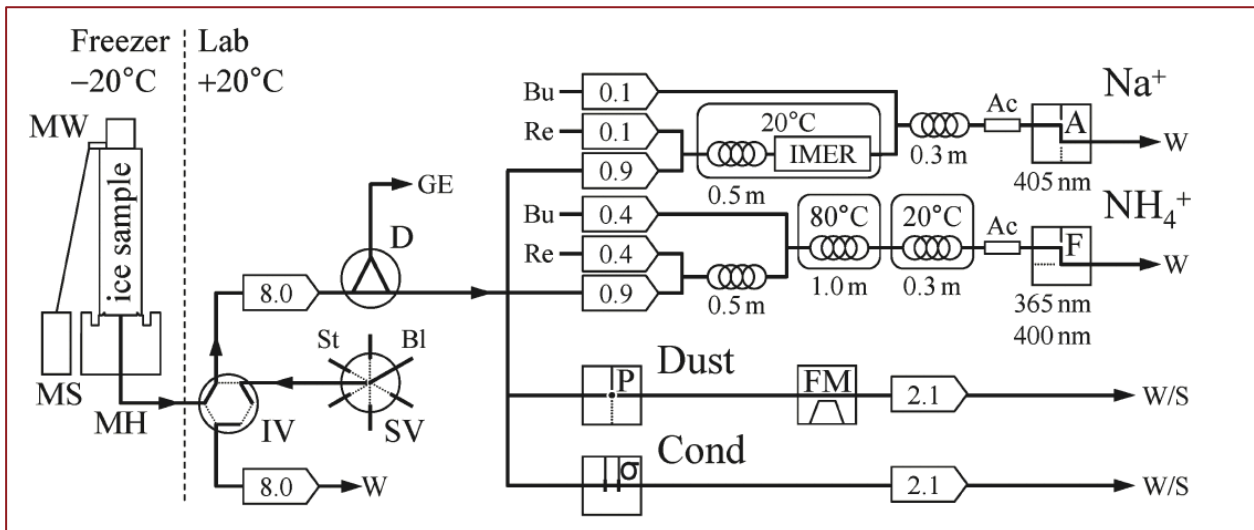


Figure 3 C CFA setup from Bigler et al., (2011) with melthead (MH), injection (IV), selection (SV), standards (St), blanks (Bl), debubbler (D), reagents (Re), buffers (Bu), discrete sampling lines (S), Accurel membrane debubblers (Ac), immobilized enzyme reactor (IMER), absorption (A), fluorescence (F), particle (P) detector, and conductivity (σ) meter.

A pump distributes the water and air into a debubbler, which reduces dispersion and prevents air entering the sampling lines (Figure 3). A degassing unit furthermore separates air and water using a gas permeable hydrophobic membrane. In chemistry measurements, a particle detector is used to detect particle size and amounts using a laser. Sodium is measured through absorbance of o-nitrophenol, a product of an enzymatic reaction in the hydrolysis of o-nitrophenyl-beta-D-galactopyranoside (ONPG) using beta-galactosidase as the catalyst (Röthlisberger, et al., 2000).

Further similar enzymatic reactions are used to provide analytical measurements. Fluorescent spectrometers with cadmium lamps are used to measure ammonium, peroxide and calcium (Sigg, et al., 1994). Nitrate is determined by absorption techniques in which reduction of nitrate to nitrite with copperized cadmium and sulfanilamide and naphthylethylenediamine (NED) (Figure 3) (Röthlisberger, et al., 2000).

The two CFA systems largely used in Antarctic and Greenland ice core studies in Europe are Bern CFA (B CFA) and Copenhagen CFA (C CFA). B CFA is configured for field deployment for subsequent testing in field conditions. The C CFA is optimized for higher resolution through slower melt rate in lab conditions (Figure 3). It is possible that 10 mm annual layers can be measured for dust, ammonium and conductivity signals based on experimental validation through NGRIP Holocene samples. Furthermore, with greater depth resolution, peaks outside of seasonal variation and multiple peaks within an annual cycle can be detected (Bigler, et al., 2011).

2.3 Ion Chromatography (IC)

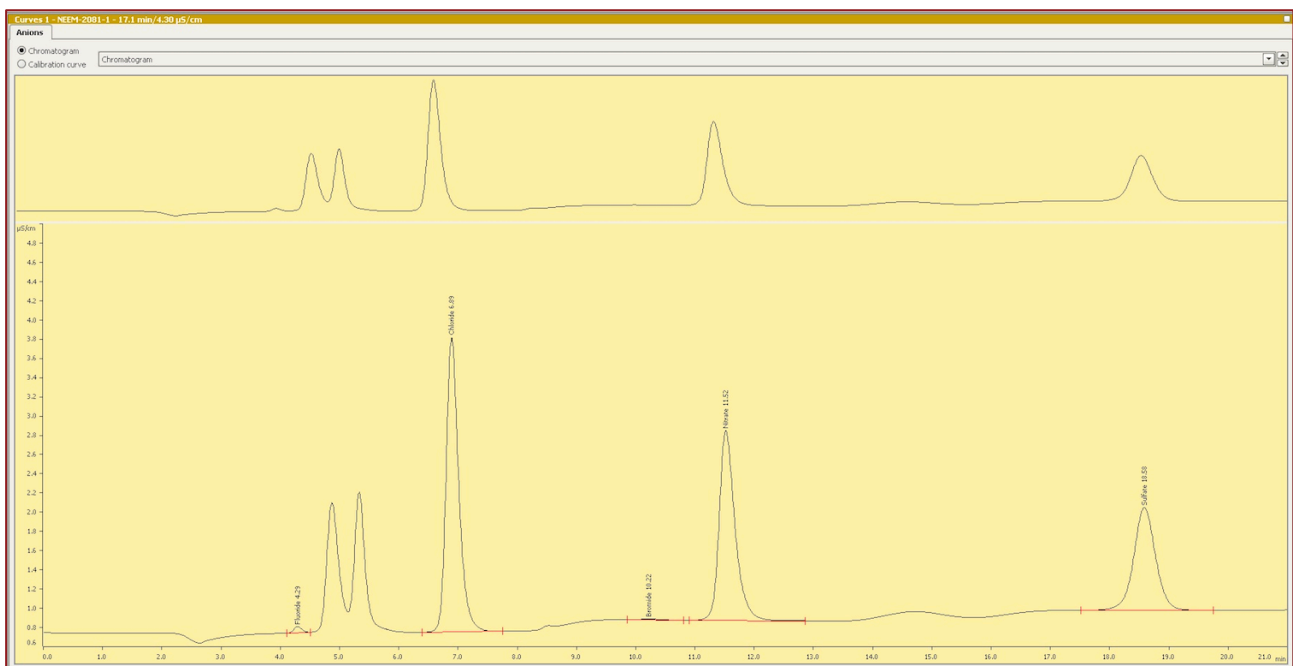


Figure 4 Example of an anion chromatogram from the IC using the ion exchange chromatography technique.

The ion exchange chromatography technique (IEC) on the ion chromatograph is fundamentally based on charges and affinities of various ions of interest with the purpose to separate charged and polar ions from each other (Kopaciewicz, et al., 1983). The guiding principle is that opposite charges have greater affinity and ions of the same charge repel each other. In cation exchange,

cations are retained in the column and the respective equivalent occurs for anion exchange. When sample is injected through the column of the ion chromatograph, ions are separated by charge through interaction between stationary and mobile phases. Cations moving through the mobile phase bind to the anion group of the stationary phase, retaining the cations. The cations are then eluted (or released) at different speeds, due to their electrostatic interactions and affinity to the anions of the stationary phase. This is done by a change in the buffer condition, such as the addition of salt. The different speeds in which targeted ions are washed out determine the retention time. The IC produces the chromatograms that plot time with conductivity in which the area of the peak is a representation of the concentration of a particular ion in the sample (Figure 4).

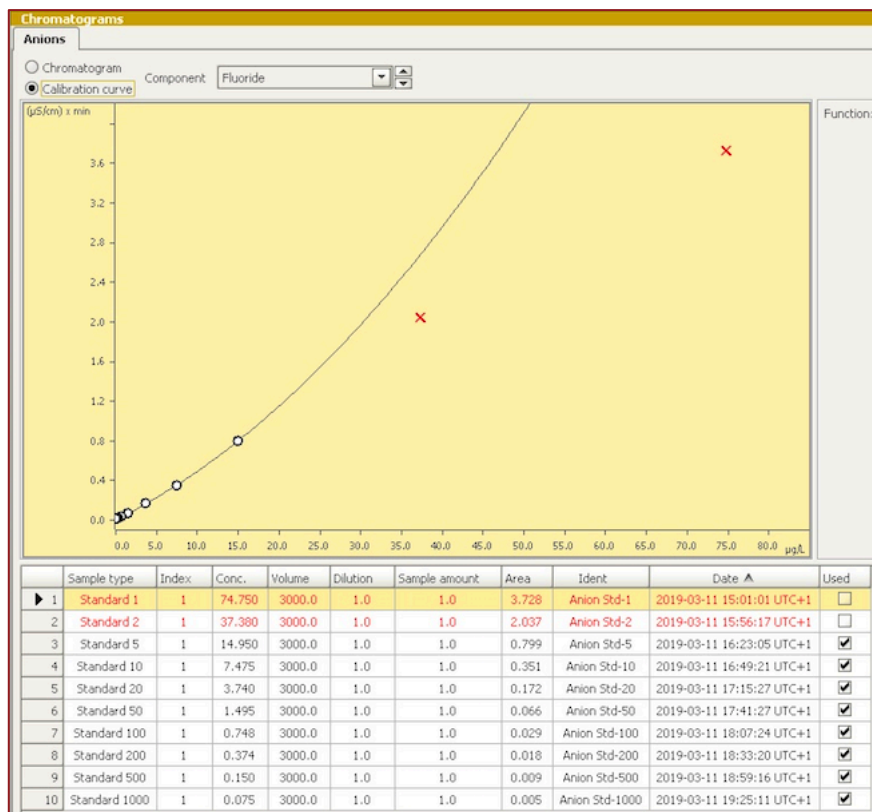


Figure 5 Example of fluoride anion calibration curve and function used to determine concentration of fluoride samples.

In order to determine concentrations of ions, calibrations are done using standards and their dilutions. Standards provide set concentrations relative to the area on the chromatogram they produce. Based on the standards of low and high concentrations, a function is created that determines the relationship between area of the peak and concentration (Figure 5). This function serves as the basis for determination of sample cation and anion concentrations and can be

customized based on the expected concentration of a samples in order to increase accuracy. For example, if lower concentrations of a particular ion is generally expected, a function can be created by favoring and emphasizing lower standard values as opposed to higher standard concentration values in order to create the best fit line through points where samples are expected to lie (Figure 5). The calibration for this study is discussed further below in the methodology.

3. The Brittle Zone (BZ)

3.1 Brittle ice



Figure 6 Example of a section of brittle ice.

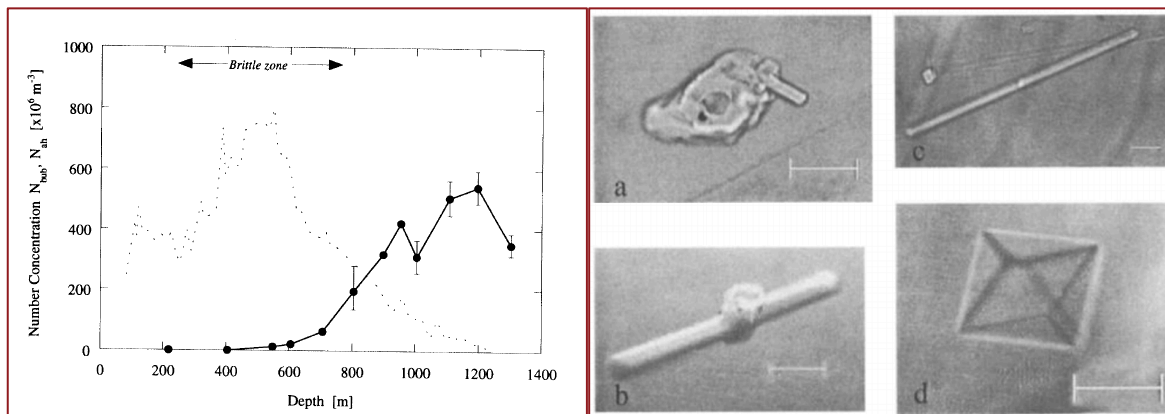


Figure 7 (left). Depth vs. number of air-hydrate crystals for Vostok, Antarctica. The brittle zone depths vary by site but all exist in the area of increasing air-hydrate crystals (Uchida et al., 1994).

Figure 8 (right). Transition of air bubbles into air-hydrate crystal in NGRIP with 100 μm scale (Kipfstuhl, et al., 2001).

The Brittle Zone (BZ) is characterized as the depth range of ice cores in which air bubbles are transitioning to air hydrate crystals (clathrates) on average at depths in ice cores between 545 and 1132 meters, varying from location to location (Figures 7 and 8) (Neff, 2014) (Uchida, et al.,

1994). Poor ice quality is most prevalent in this zone due to fast decompression of ice cores at surface, resulting in fracturing and drill liquid contamination (Figure 6). As ice is retrieved from a high pressure environment and exposed to atmospheric pressure, the pressure of internal air bubbles exceed that of the surrounding environment, resulting in cracking. With increasing depth, the number of air bubbles decrease and clathrates increase. The BZ ends when most or all air bubbles become clathrates (Figures 7 and 8).

The depth of the BZ is largely dependent on accumulation and air surface temperature, which in turn affects densification (Neff, 2014) (Uchida, et al., 1994). Thickness and density of firn has implications on the pressure imposed on air bubbles at depth and affects the depths where fractures are most prone to occur. In locations of warmer, higher accumulation rates, brittleness is relatively more severe as firn reaches ice density quicker and there is greater burden for air bubbles. With lower surface temperatures, BZ ends at shallower depths. EPICA Dome C, characterized by low accumulation, the brittle zone corresponds to ages between 29 and 80.5 ka BP. Contrastingly, the NEEM ice core brittle zone corresponds to 3.5-7 ka BP. In addition to accumulation and temperature, number of air bubbles, size, micro-bubbles, grain size and crystal anisotropy also play a role in the formation of the brittle zone and transition to clathrates.

The tendency of ice in this zone to fracture and crack creates several difficulties, including inaccuracies in calculating depths and observing physical properties (Neff, 2014). The brittle ice is difficult to process for transport, often exacerbating contamination. Furthermore, analysis of ice cores is significantly hindered due to ice quality. Continuous flow analysis (CFA) is not feasible for analysis of impurities due to contamination of water lines that resides and impacts the analysis of subsequent samples.

To improve the quality of ice in the BZ, drilling technique and ice handling during processing are influential. Techniques that can allow a more steady, gradual transition from in situ pressure to atmospheric pressure can reduce the extent of fracture. Storage of the ice at temperatures similar to that at depth of the borehole can furthermore help. At present, brittle ice is also left for a year in the field to relax and overwinter, allowing the pressurized air bubbles to equilibrate prior to processing (Neff, 2014).

3.2 Drill liquid

There are certain necessary requirements for drill liquids, including density, viscosity and compatibility with ice and surroundings (Sheldon, et al., 2014). Pressure exerted by the fluid on the borehole is affected by the density of drill liquids. The desired density between 920-950 kg m⁻³ between -10 to -32 °C helps minimize the stress place on ice cores. Particularly in deep ice drilling, time for the drill to descend, drill, and ascend is critical in determining how long and how many seasons an operation requires. Fluid viscosity influences the drill travel speed. Furthermore, drill liquid fluid must have a minimal or no effect on the ice chemistry in addition to adjacent machines and working site (Sheldon, et al., 2014).

The use of a blend of Estisol 240 and Coasol increased drill speed with a relatively larger borehole. Estisol 240 is derived from coconut oil and is a strong solvent, similar to that seen in industrial cleaning fluids and degreasers (Talalay, 2011). Coasol is a di-butyl ester that is commonly used as a coalescing agent and is also a strong solvent. Together, they have low vapor pressure, biodegradability, no odor and less toxicity. The use of this mixture of drilling fluids increased success of ice retrieval in warmer conditions in the ice sheet (Sheldon, et al., 2014).

4. Integration of CFA and IC methods for chemistry

4.1 Sampling of NEEM BZ

The NEEM BZ extends from the depth of about 740 -1150 meters. The ice was cut into CFA pieces of about 55 cm long each and stored in ice core boxes that hold about 50 bags. Due to poor ice quality, sampling could not be conducted at regular intervals without selection bias. Rather, visual assessment was made of each bag and the bags most suitable for CFA melting were selected, up to 5 bags per box. The bags most suited for CFA melting had to have relatively fewer cracks in which drill liquid could have penetrated sample. Furthermore, each bag had sections of greater than 10 cm which increases the chances of producing real data and data signals free of contamination from handling and drill liquid. In preparation for melting, sampling pieces greater than 10 cm and free of cracks were cut into 33x33 cm, measured for length, dusted off and placed into frames.

4.2 CFA for NEEM BZ

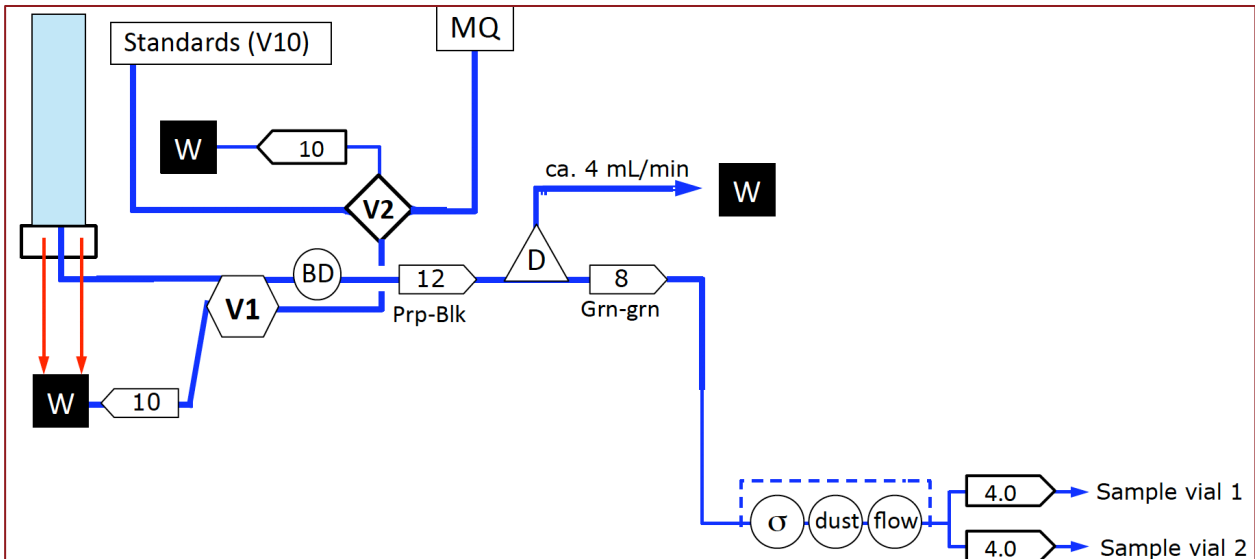


Figure 9 CFA configuration for measurements and collection of discrete samples of NEEM BZ with bubble detector (BD), injection valves (V1 and V2), debubbler (D), waste (W), and conductivity (σ).

The use of CFA to melt sample was an effort to decrease contamination and collect discrete samples that could be used for IEC. The CFA system was reorganized and simplified to measure for conductivity and dust and to collect discrete samples (Figure 9).

A 33 x 33 mm ice sample was placed in the melthead where sample was injected through the bubble detector and through the two injection valves (V1 and V2) (Figure 9). Sample flowed out of the bubble detector at 12 mL/min and into the debubbler where 4 mL/min went to waste and the rest was analyzed for conductivity and dust.

The Klotz GmbH Abakus uses the sensor type LDS-12/25 to measure the amount of dust in a sample based on light impedance. As a particle passed through a flow cell, a “shadow” was created and that “light extinction” was measured to determine the size of the particle and the number of them (Simonsen, et al., 2018). The conductivity meter measured the ionic imbalance, the number of ions with free electrons. The signal was then translated to an electrical signal observed as $\mu\text{S}/\text{cm}$.

Sample flowed into 2 vials that were collected approximately every 10 mL with the effort to keep contamination from entering by disconnecting discrete sampling close to breaks where contaminated ends may melt and enter vials. A set of two vials of discrete samples was collected at a time and frozen.

4.3 Ion Chromatography (IC) of BZ

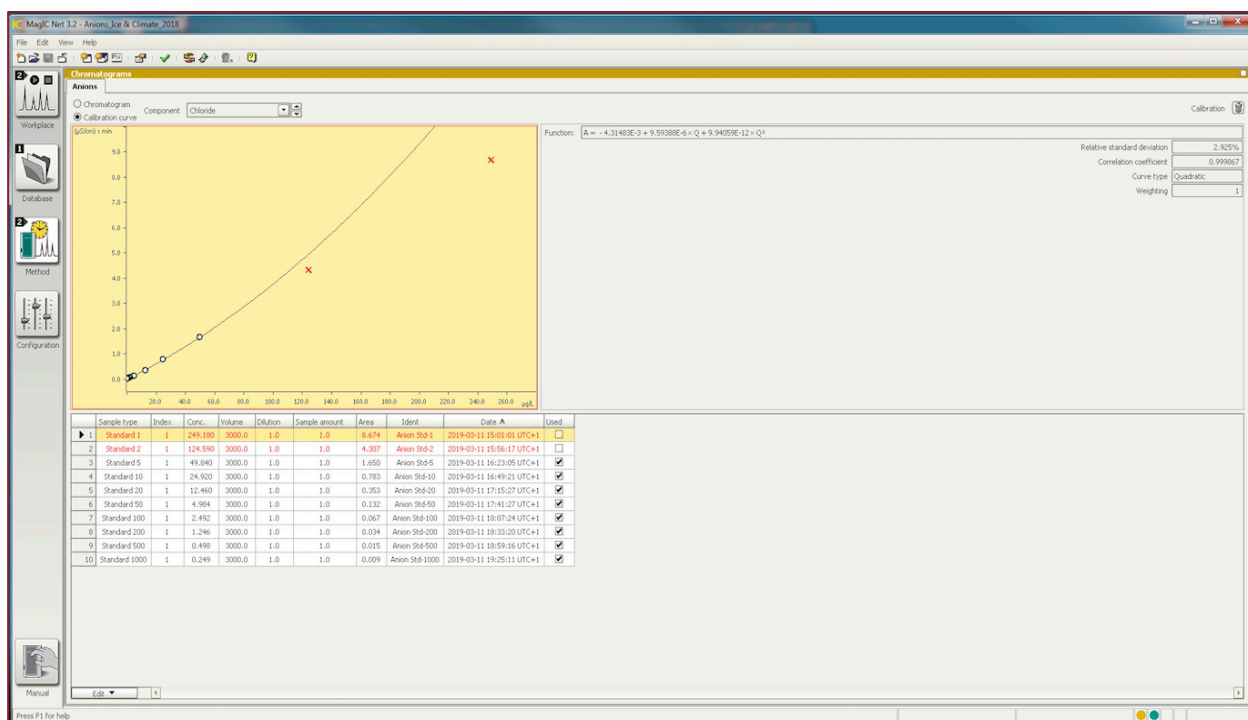


Figure 10. IC calibration curve for chloride ions. Standards 1 and 2 (red) were excluded in calibrations to create a more accurate function that reflects the expected sample IC values for chloride in Greenland. Similar curves were made for other tested ions.

The cations analyzed on the IC include lithium, sodium, ammonium, potassium, calcium, and magnesium and anions include fluoride, chloride, bromide, nitrate, and sulfate. The Metrohm Ion Chromatograph using the IEC technique was calibrated using cation and anion standards which were used to set retention times, area and concentration. Then, calibration curves based on the relationship between concentration and area were made using standard data. An equation of the line of best fit was calculated using linear or quadratic relationship (Figure 10). The equation of the calibration curve was customized to fit the data to produce the most accurate concentration values based on area. This was done by selecting (de-selecting) the values in which the line should fit. For example, Cl⁻ values measured in Greenland ice are not expected to reach the levels measured in Standards 1 and 2. Therefore, these standards are excluded from the line-of-best-fit calculation to create a curve that best suits the points in which Cl⁻ concentrations are most likely to lie. This increases the accuracy of concentration values (Figure 10). The vial samples were then placed onto the IC tray and measured through IEC for chemistry. The output concentrations were presented in chromatographs and datasheets with retention time, area and concentration.

4.4 CFA and IC data processing

The CFA output data provided conductivity and dust data for each bag. Using the Matlab program, the data were plotted with respect to acquisition time and the data corresponding to the period in which vial sampling took place was highlighted. After initial visual inspection of the data, the relative depth (~0-0.55 m) was calculated for each bag using the data produced by the laser encoder that measures meltrate at each timestep. Breaks in each bag were inserted into the relative depth calculation using the measurements noted in the cutting log. The resulting calculations were about a centimeter of the visual measurement noted on the cutting log. Absolute depth was calculated knowing the start depth of each bag and the calculated relative depth of the core, including the breaks.

The cation and anion data from the IC provided concentrations of the aforementioned ions. Each sample consisted of part or the whole piece of a bag. By digitally marking the instances in which vial sampling began and stopped during CFA, the known length of ice of each IC vial and the absolute depth of which the sample derives from could be calculated. The start and end depths of the each sample along concentrations were plotted. In order to plot cation and anion concentrations by time, the depth-age scale by (Rasmussen, et al., 2013) was used. The interpolation of the depth provided the output of age. The information compiled has thus far provided dust, conductivity, depth, age and concentrations of various cation and anion species that together serve as proxies to climate during the Holocene.

NEEM isotope data was provided by the NEEM isotope consortium at the Physics of Ice, Climate and Earth (PICE) at the University of Copenhagen. The isotope data was smoothed and plotted for the corresponding depths and juxtaposed with the cation and anion IC data. Because of the approximately 3000 year timespan of the dataset, the cation and anion data were further separated into 4 periods for overall better visualization.

In order to determine if the produced IC data is of true value and relevance, comparisons had to be done with already published data. This included data from Schüpbach et al. (2018) and Spolaor et al. (2016), both of which have datasets for the NEEM ice core, either before, after, or slightly overlapping with the end of the BZ. The parameters from Schüpbach et al. (2018) included ammonium, nitrate, sodium, calcium and sulfate. Bromide data was provided by Spolaor et al. (2016). Because Schüpbach et al. (2018) only had data overlapping with the IC

data at approximately 7200-7400 years B2K (~1135-1152 m), the only comparison possible was at that coinciding period. More values from the Schüpbach et al. (2018) dataset were included than what was in the IC data in order to see further trends and create more balanced and true average values. The Schüpbach et al. (2018) data for the stated ions were plotted in comparison with corresponding IC concentrations. Mean values from the Schüpbach et al. (2018) data were used to understand the range of the IC concentrations relative to the published dataset. Bromide data was only available before and after the area of interest for comparison (the IC concentrations). Therefore, values from Spolaor et al. (2016) before and after the BZ were plotted with the IC concentrations for the BZ period.

Furthermore, a comparison was done for NH_4^+ using values from GISP2 to provide insight from values not only from NEEM. Mean and standard deviation values were calculated for the overlapping period corresponding to the NEEM BZ and also for the entire Holocene. GISP2 data provided a continuous dataset that included all the depths of which correspond to the NEEM BZ and the use of NH_4^+ for comparison was on the basis that it is a more understood parameter. Comparison of IC data to other cations and anions at GISP2 can also be done in the future.

On a large scale visualization of the IC data, some areas of interest were noted. These consisted of areas in which one or more of the IC anion or cation concentrations were relatively higher, leading to further curiosity to see the visualization on a small scale. Bags 1475 (810 m), 1610 (~885 m), 1679 (~923m), 1728 (~949.5 m) 1733 (~950 m), 1826 (~1003 m), 1835 (~1009 m) and 2077 (1142 m) were cases in which a more detailed analysis was conducted. NEEM ECM and DEP data were used in each of these cases to compare and validate the produced CFA conductivity results for the BZ.

5. Results

5.1 IC chemistry results with depth and time

IC chemistry data with depth (m)

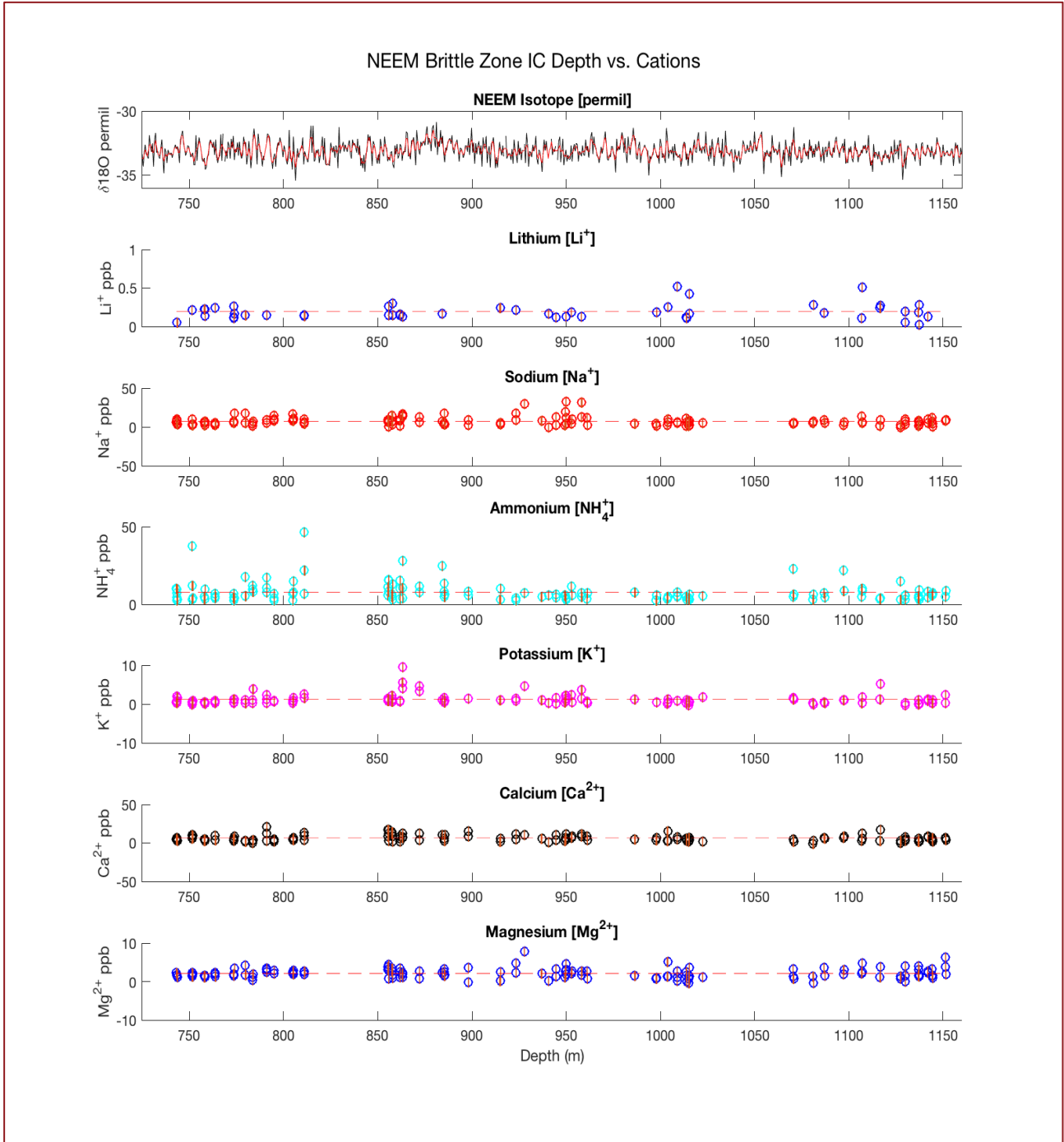


Figure 11: Depth (m) vs. Cations from ion exchange chromatography results.

The resulting cation data from the IC is shown on a depth scale. Each sampling point includes marks that demonstrate the average concentration over a depth increment. Dashed lines are

indicative of the mean concentration of all samples for a given ion. Stable waster isotope data from the corresponding depths are also present on the top panel, in which the red line is indicative of smoothed data. While vial indicators are not visible on this large scale graph, they are in the graphs that follow.

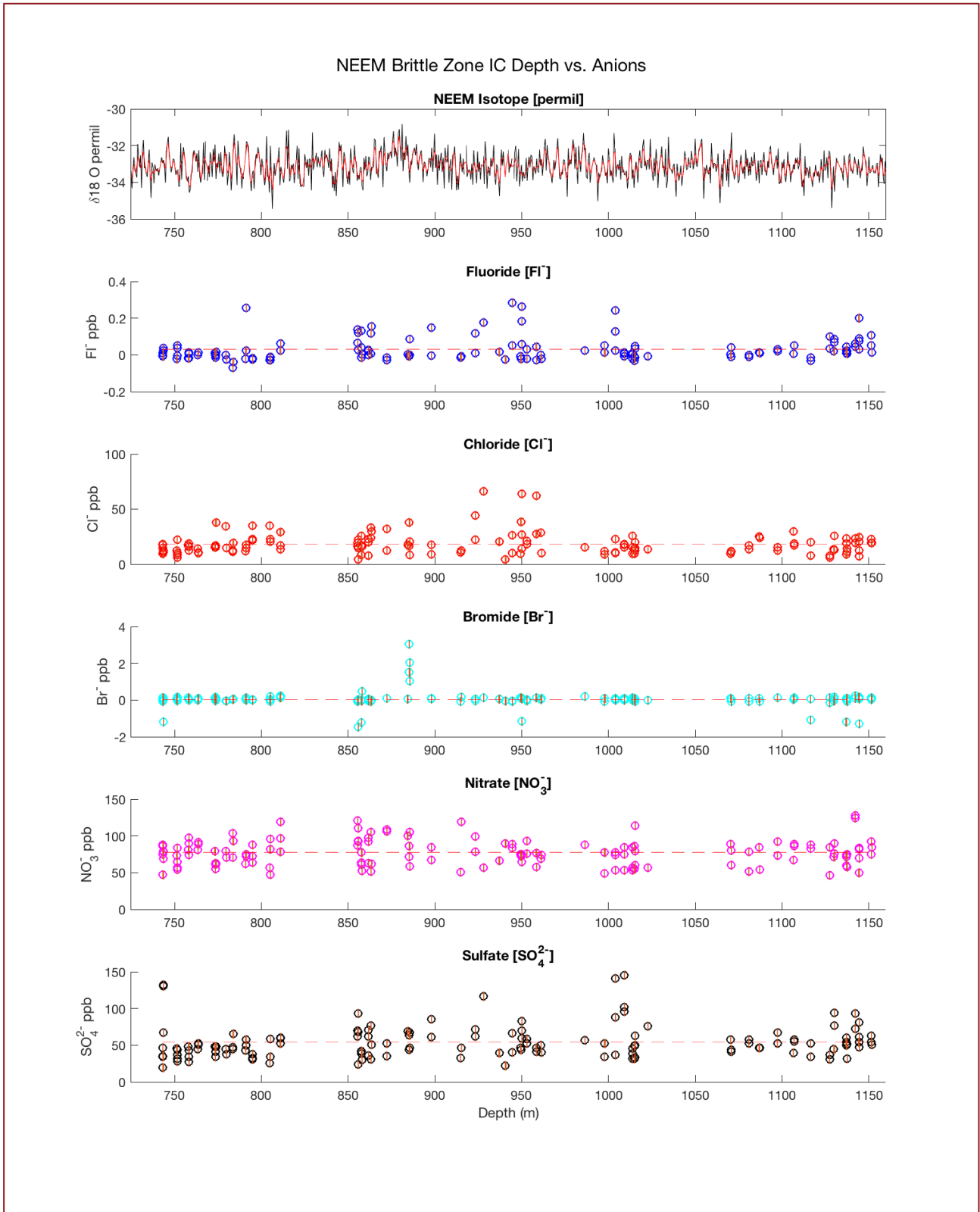


Figure 12 Depth (m) vs. anions from ion exchange chromatography results.

The resulting anion data from the IC is shown on a depth scale. Each sampling point includes marks that demonstrate the average concentration over a depth increment. Dashed line is indicative of the mean concentration of all samples of a given ion. Stable water isotope data from the corresponding depths are also present on the top panel.

IC chemistry data with time (years B2K)

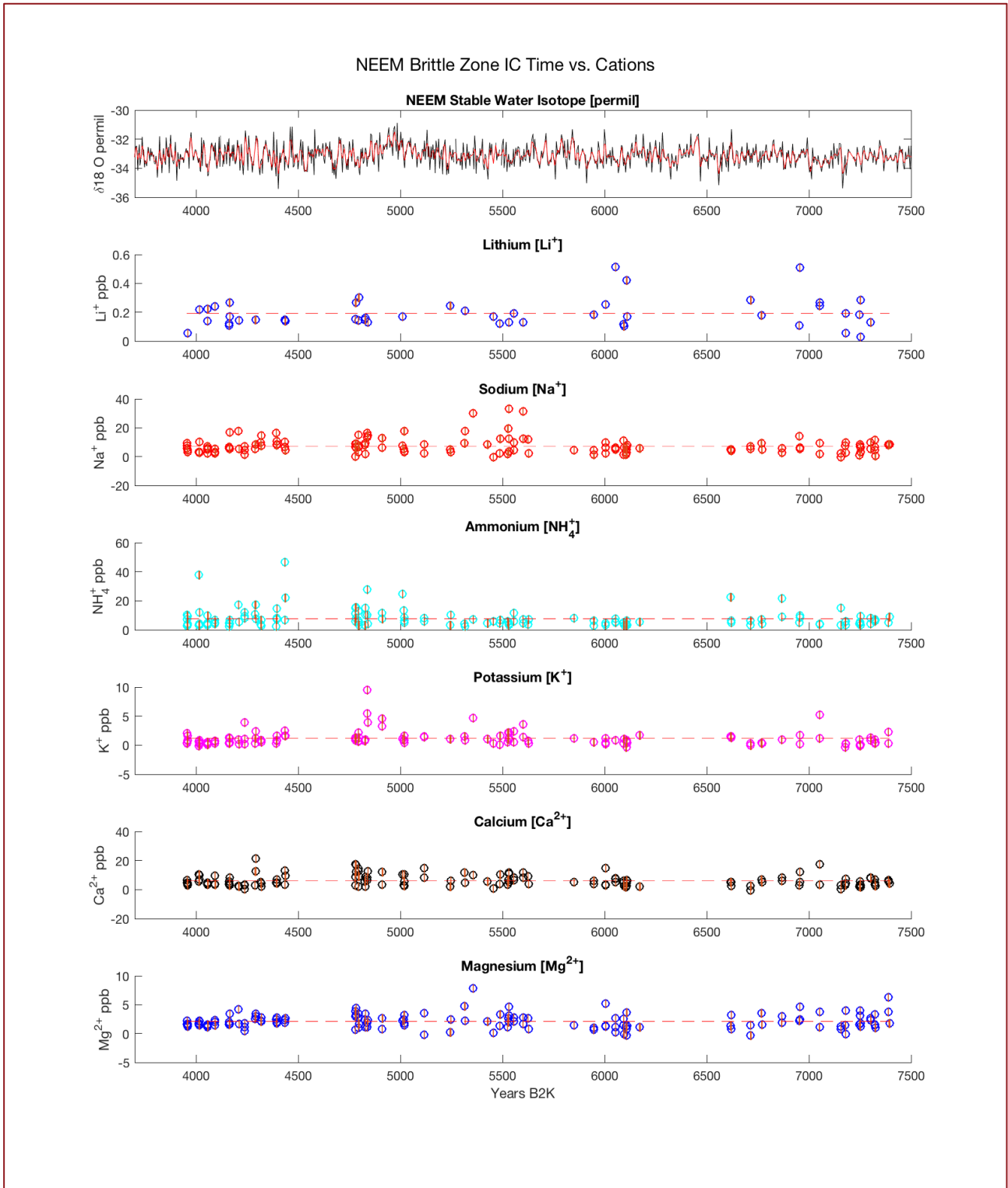


Figure 13 Time (years B2K) vs. cations from the ion exchange chromatography results.

The cation concentrations of all samples are graphed according to time, with marks that demonstrate the average concentration over a time period. Dashed lines are indicative of mean

concentration of all samples for a given ion. Stable water isotope data from the corresponding time are also present on the top panel.

The age data is produced through interpolation using Rasmussen et al. (2013) time scale for NEEM and the calculated depths of the samples done in this study. The calculated depth for each sampled IC vial is matched to the corresponding depth in the Rasmussen et al. (2013) to retrieve age data.

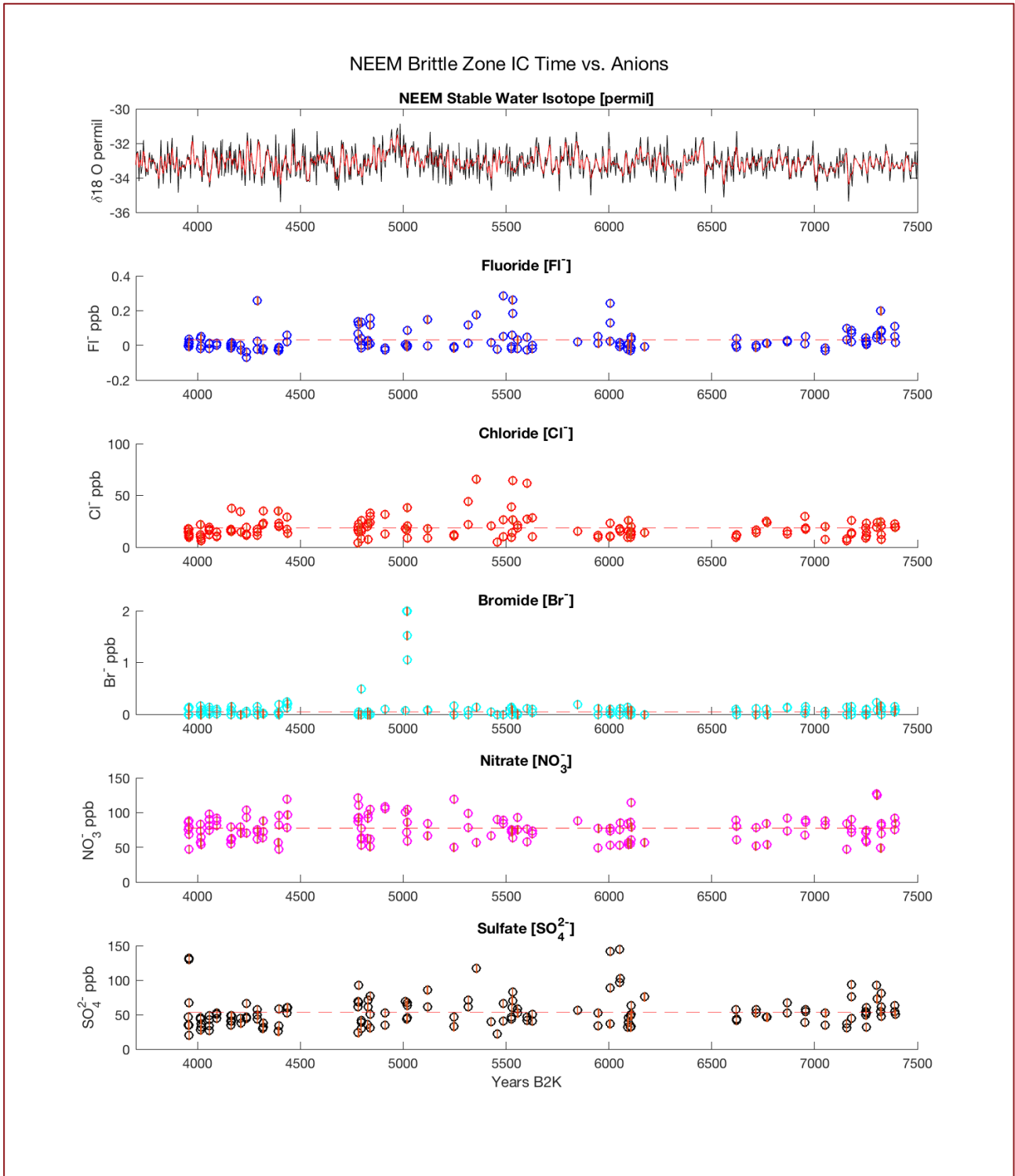


Figure 14 Time (years B2K) vs. anions from ion exchange chromatography results.

The anions concentration of all samples is graphed according to time, with marks that demonstrate the average concentration over a time period. Dashed lines are indicative of the mean concentration of all samples for a given ion. Stable water isotope data from the corresponding time period are also present on the top panel.

Table 2. Table of means and standard deviations (SD) of concentrations from IEC of each cation species based on 138 samples.

Cation	Mean (ppb)	SD
Lithium (Li⁺)	0.1914	0.0978
Sodium (Na⁺)	7.3529	5.4888
Ammonium (NH₄⁺)	7.6764	6.3010
Potassium (K⁺)	1.1607	1.3046
Calcium (Ca²⁺)	6.2047	3.9653
Magnesium (Mg²⁺)	2.1185	1.2644

Table 3. Table of means and standard deviations (SD) of concentrations from IEC of each anion species based on 138 samples.

Anion	Mean (ppb)	SD
Fluoride (F⁻)	0.0310	0.0635
Chloride (Cl⁻)	18.4847	10.1856
Bromide (Br⁻)*	0.0411	0.4641
Nitrate (NO₃⁻)	77.5118	17.4969
Sulfate (SO₄²⁻)	53.7884	22.5793

**Disproportionately high values of bromide, likely due to contamination, have distorted the mean and SD.*

5.2 IC chemistry results split by time (years B2K)

For a more concentrated view, the timespan of the sampling points is split into 4 parts based on where there are gaps in which there are no data points. The resulting plots show cation concentrations followed by anion concentrations, both of which are in 4 graphs in chronological order (Panels 1-4).

Cations Panels 1-4

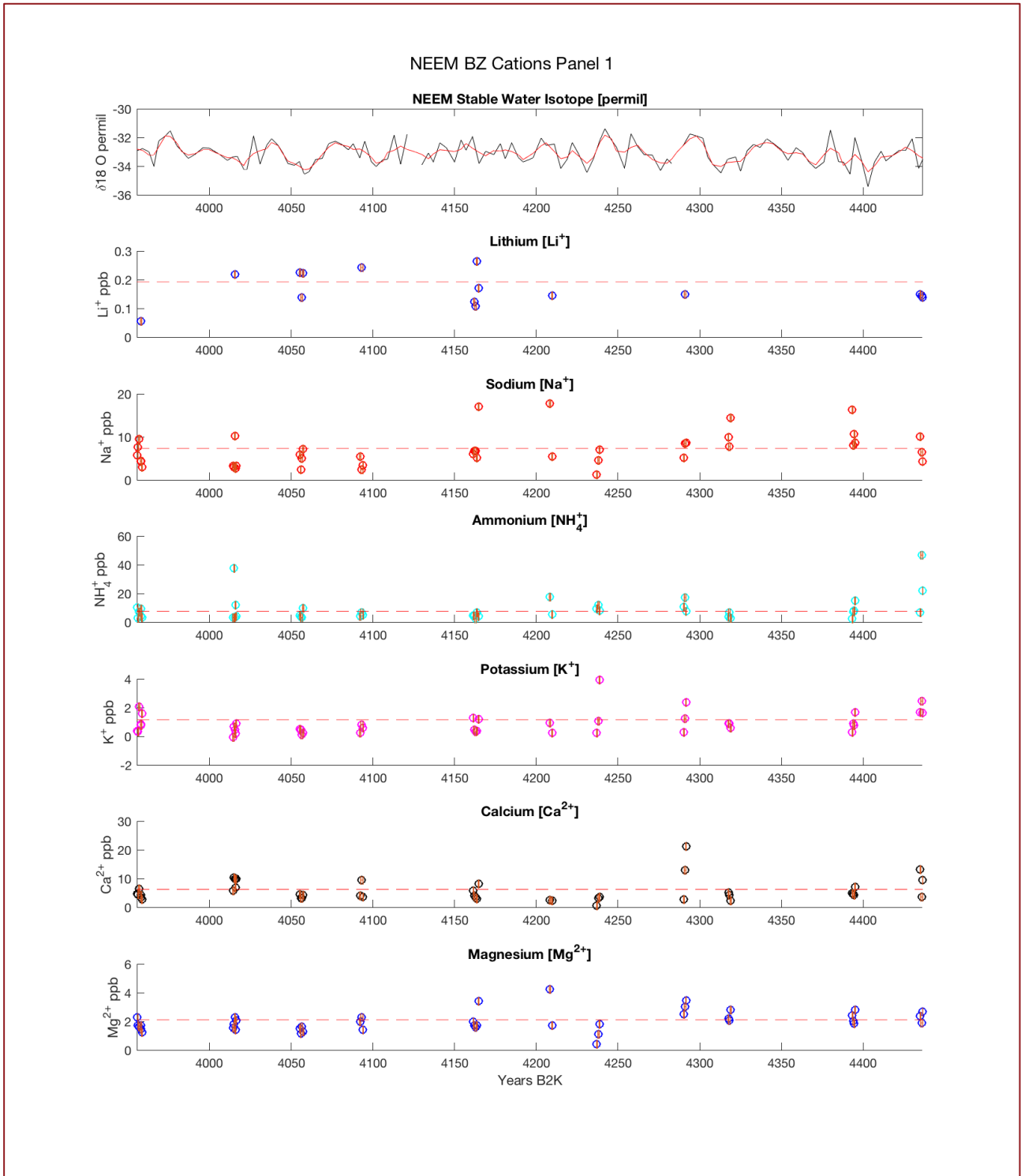


Figure 15 Cations Panel 1 split by time (years B2K).

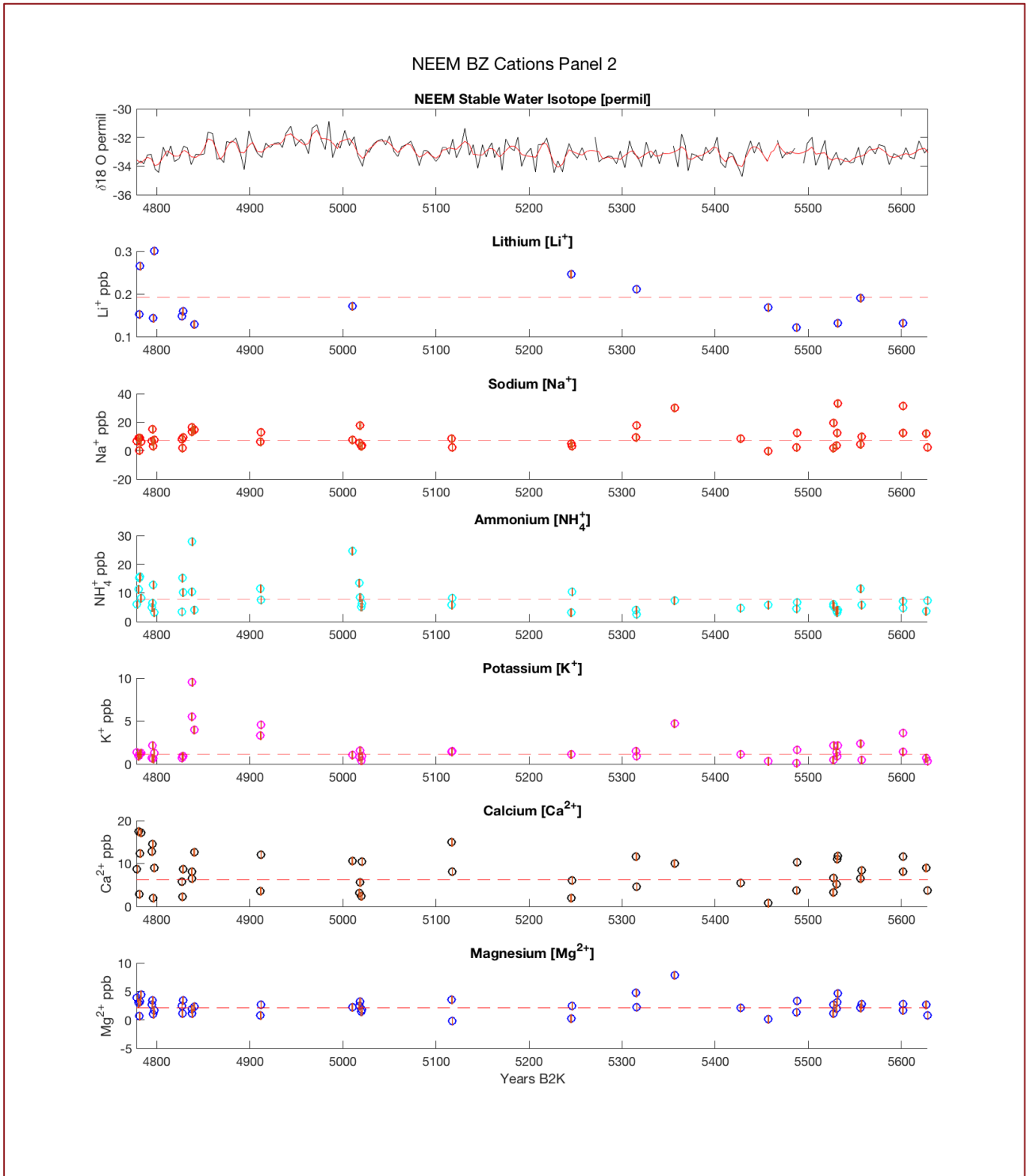


Figure 16 Cations Panel 2 split by time (years B2K).

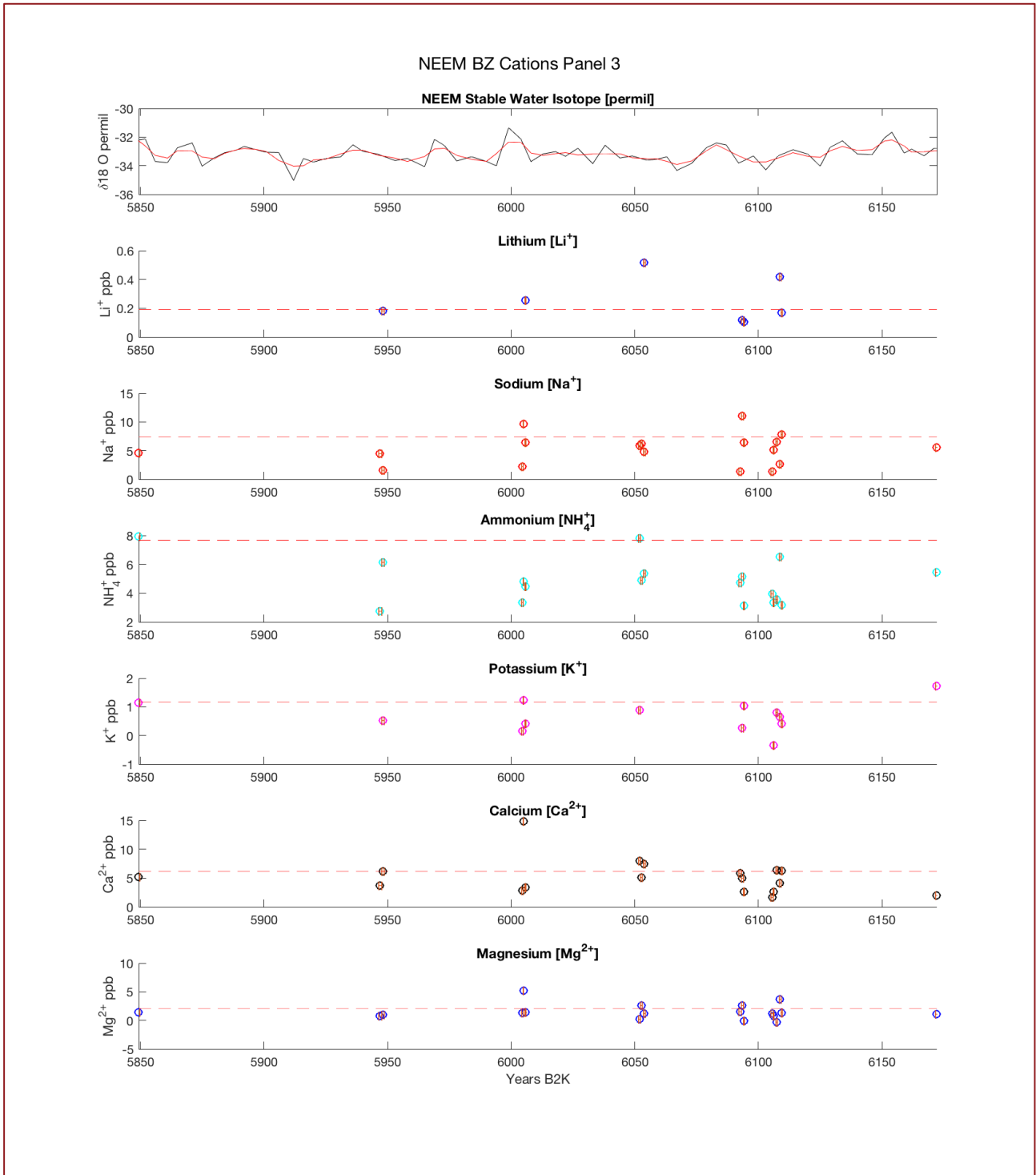


Figure 17 Cations Panel 3, split by time (years B2K).

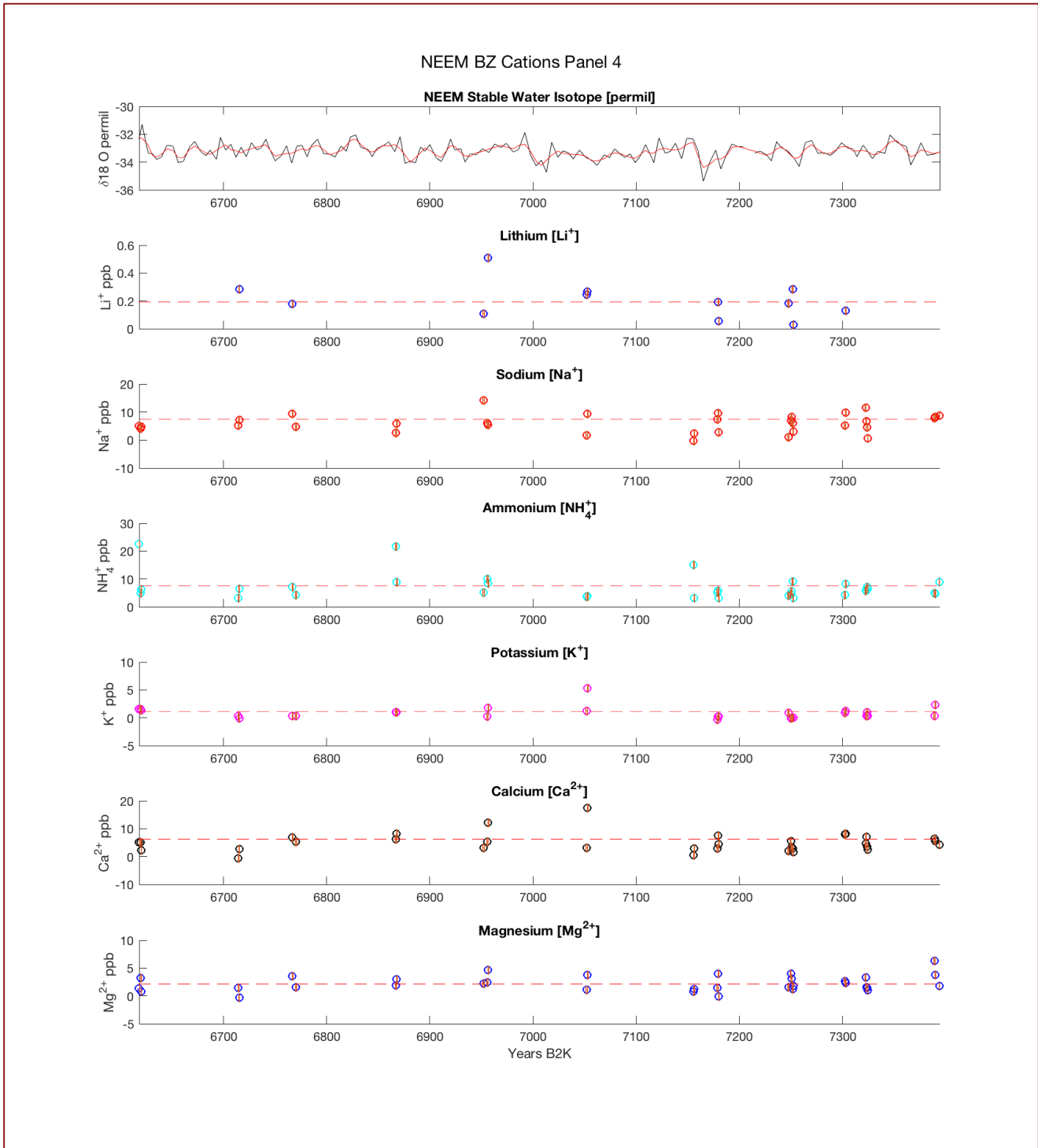


Figure 18 Cations Panel 4, split by time (years B2K).

Anions Panels 1-4

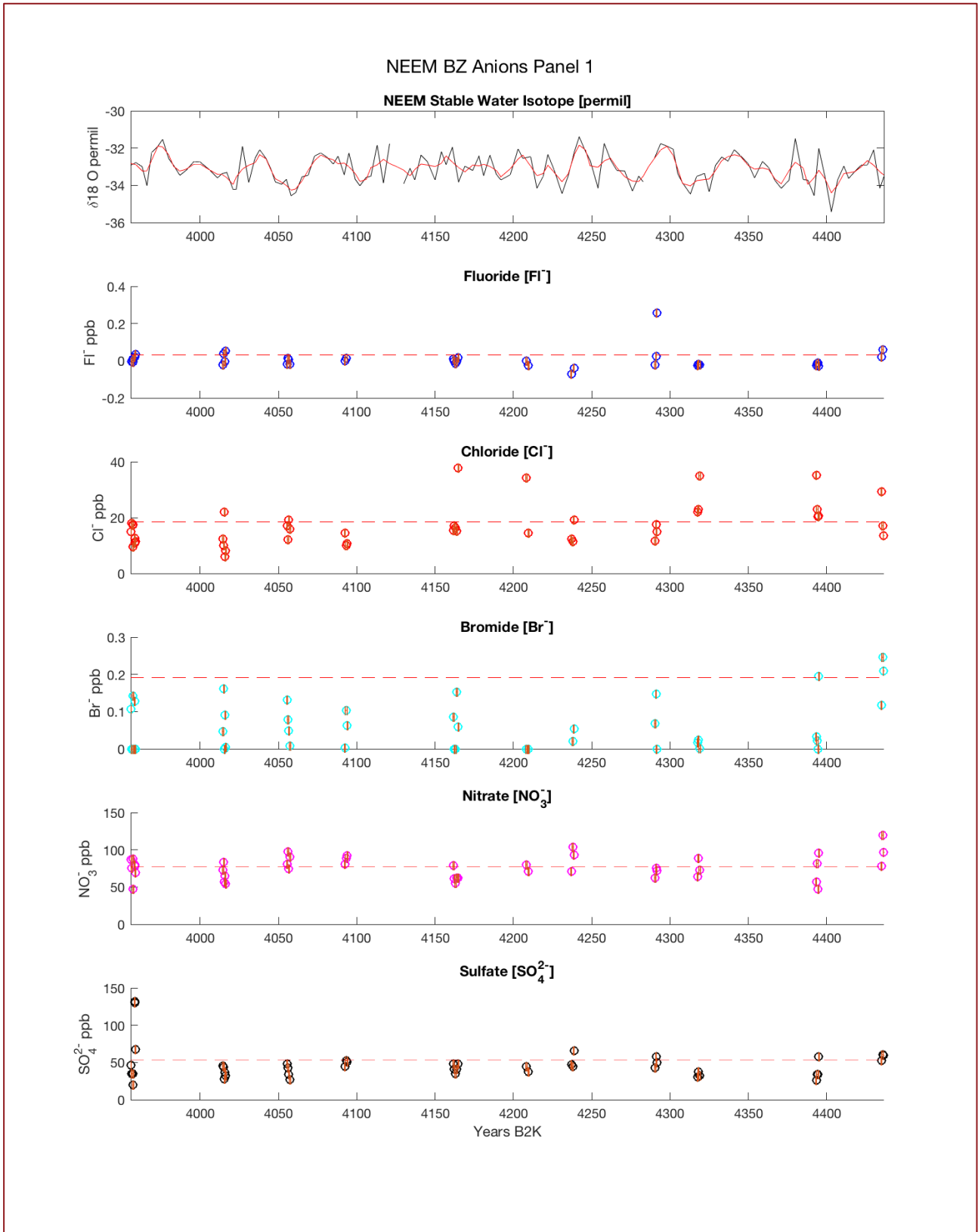


Figure 19 Anions Panel 1, split by time (years B2K).

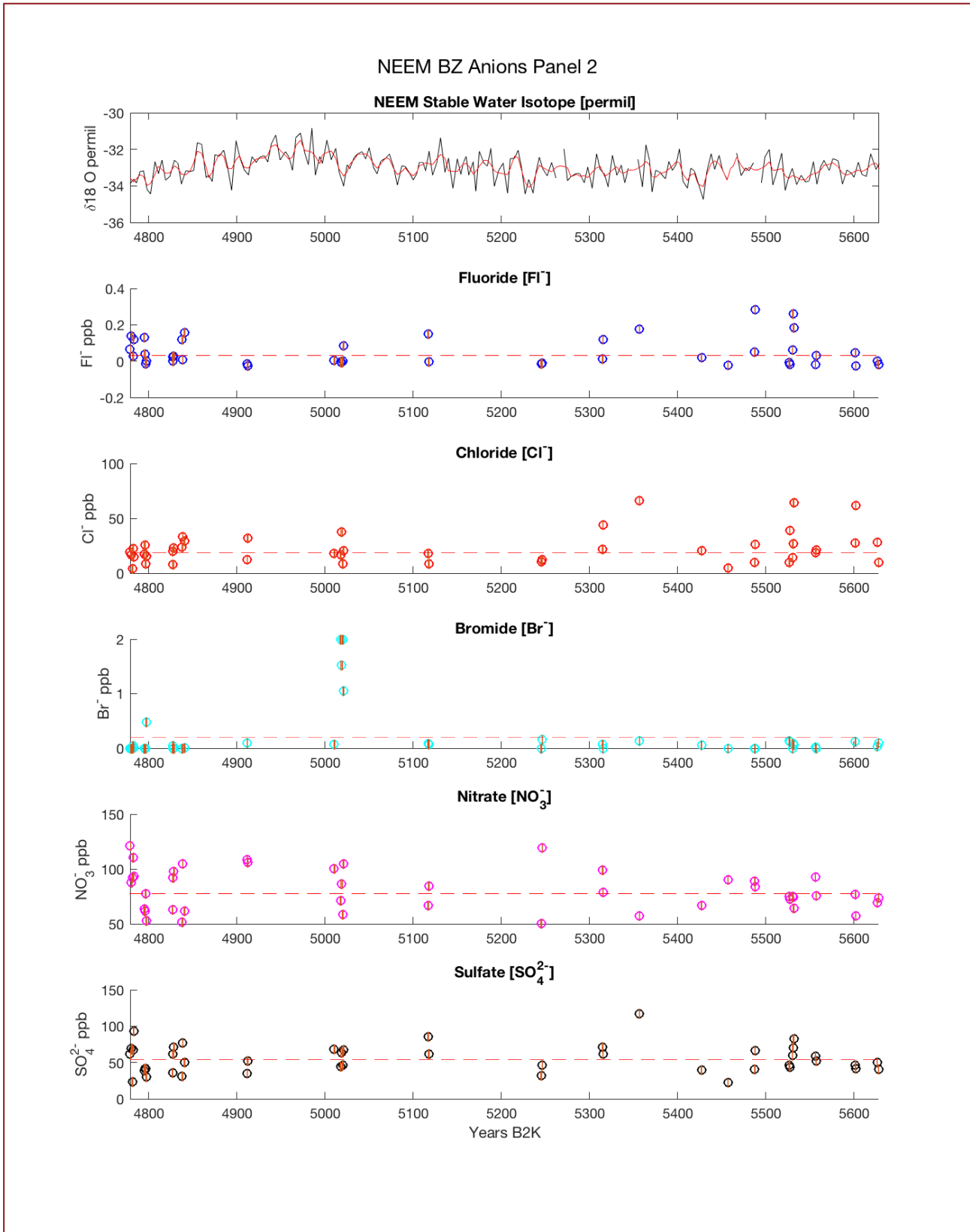


Figure 20 Anions Panel 2, split by time (years B2K).

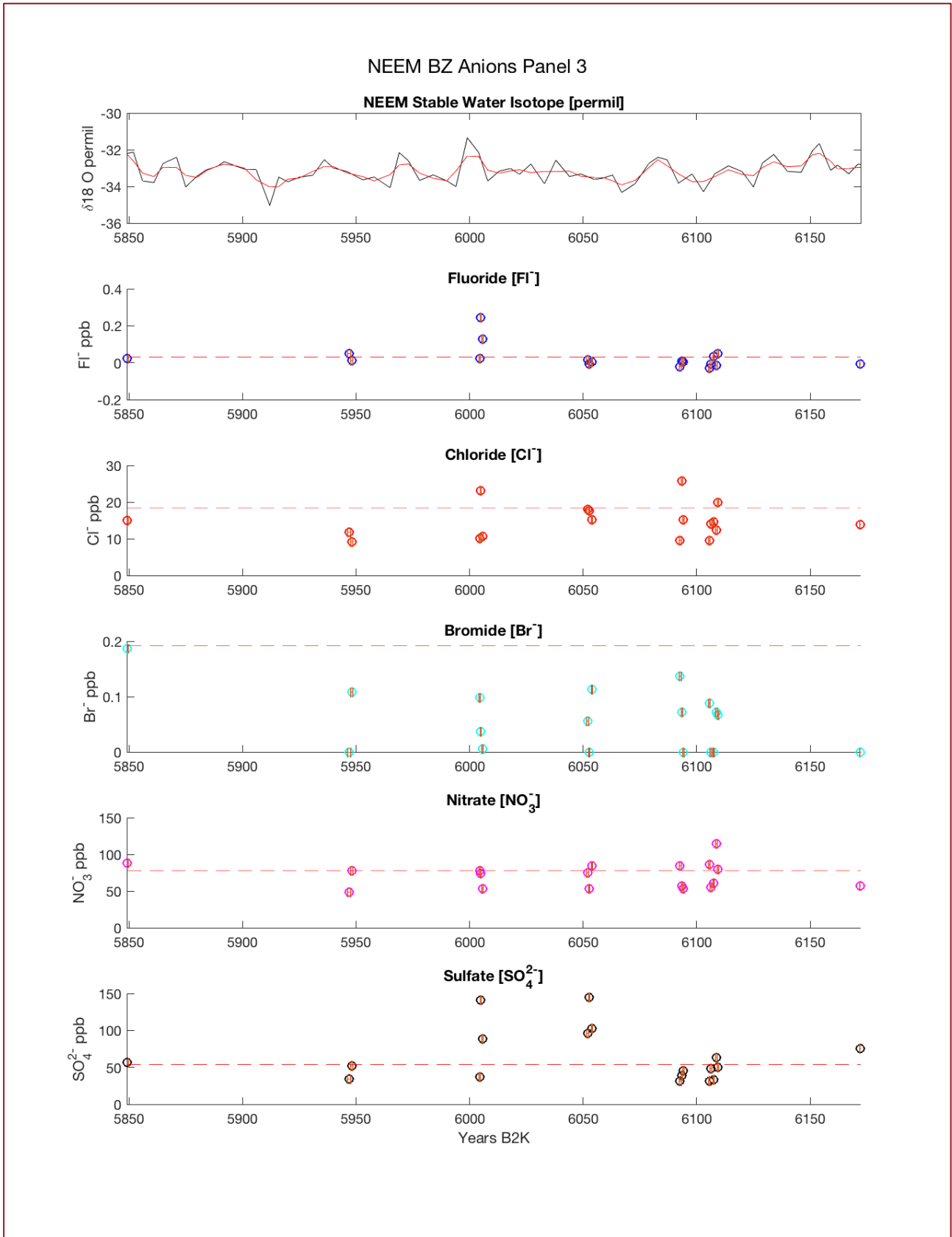


Figure 21 Anions Panel 3 split by time (years B2K).

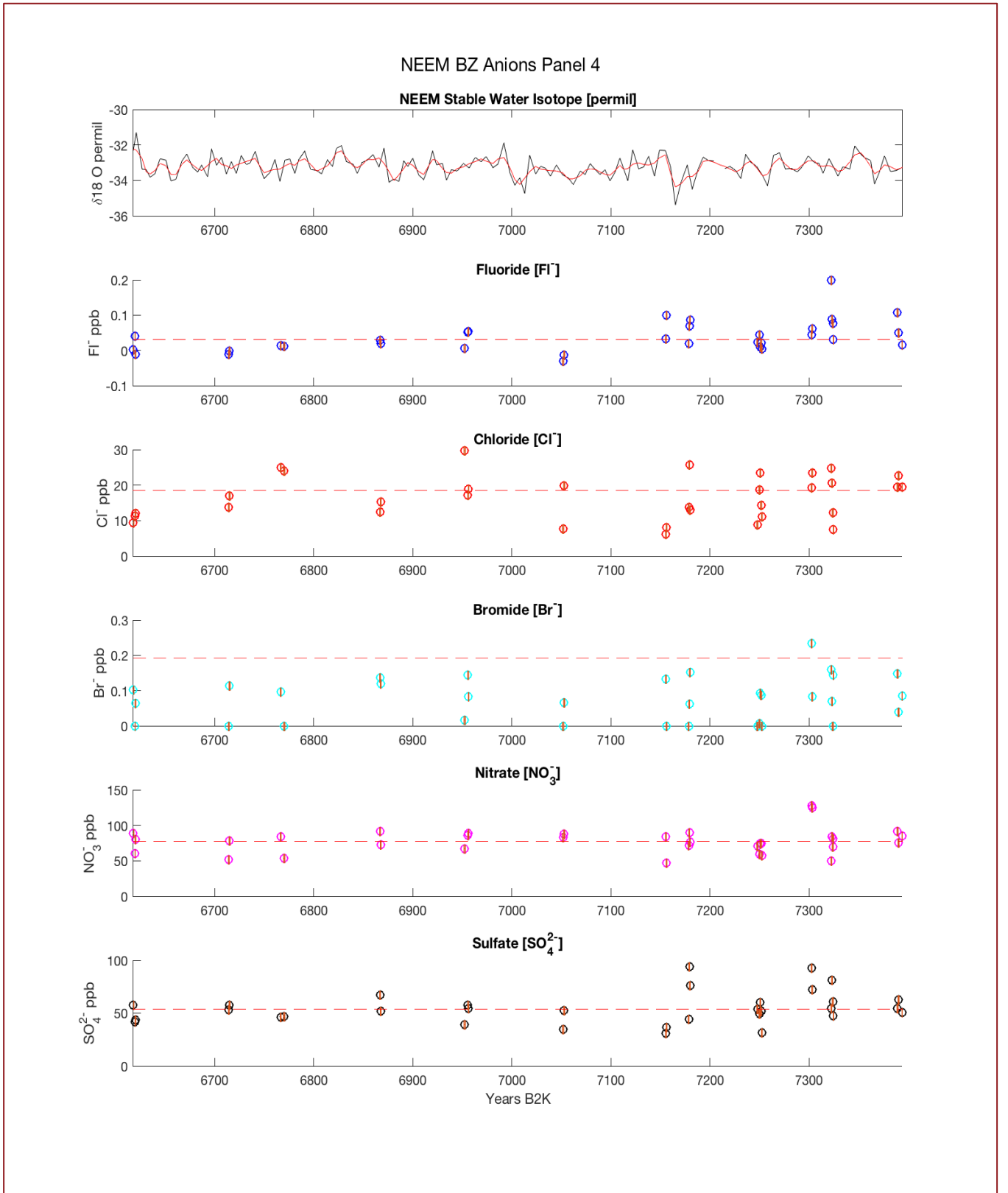


Figure 22 Anions Panel 4 split by time (years B2K).

5.3 Comparison of NH_4^+ , NO_3^- , Na^+ and Ca^{2+} values

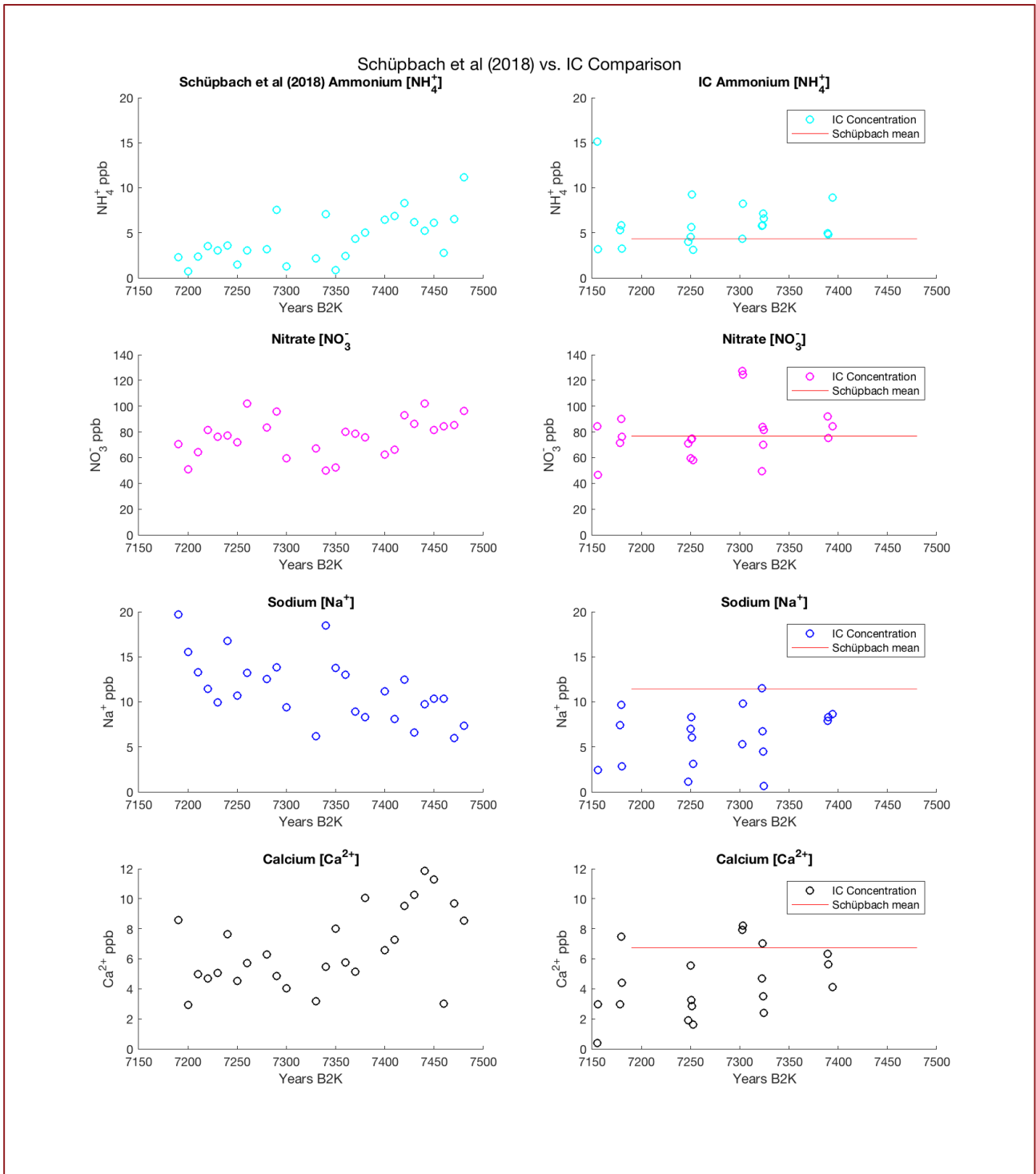


Figure 23 Comparison of IC values with that of Schüpbach et al (2018) for NH_4^+ , NO_3^- , Na^+ and Ca^{2+}

The common ionic parameters measured on the IC and present in Schüpbach et al. (2018) are compared. The concentrations of the published dataset derive from CFA at 10-year resolution. However, because CFA was not done in the BZ, there are only a few data points in which the IC

data and Schüpbach et al. (2018) have in common. A comparison is still carried out, with a few additional points from Schüpbach included to create a more conclusive average.

The left column consists of the ion concentrations from the sampling area of interest in Schüpbach et al. 2018 (Figure 23). The mean from the portion of the Schüpbach et al. (2018) dataset used is plotted with the IC data in the form of a red line in order to visualize the range of where the IC concentrations lie relative to the already published data. The mean is plotted in the respective time in which the published data corresponds to, as the comparison of published data and IC data do not perfectly coincide in time.

Table 4. Table of comparison of means and standard deviations (SD) between the range of Schüpbach et al. (2018) used for comparison and IC-produced data.

Ion	Schüpbach et al (2018) mean (ppb)	SD (Schüpbach et al 2018)	IC mean (ppb)	SD (IC)
Ammonium (NH₄⁺)	4.3547	2.6124	6.0896	2.8287
Nitrate (NO₃⁻)	76.6834	14.8433	78.7120	20.8238
Sodium (Na⁺)	11.4132	3.5879	5.8392	3.3881
Calcium (Ca²⁺)	6.7316	2.6056	4.3789	2.2715

5.4 Comparison of SO_4^{2-} values

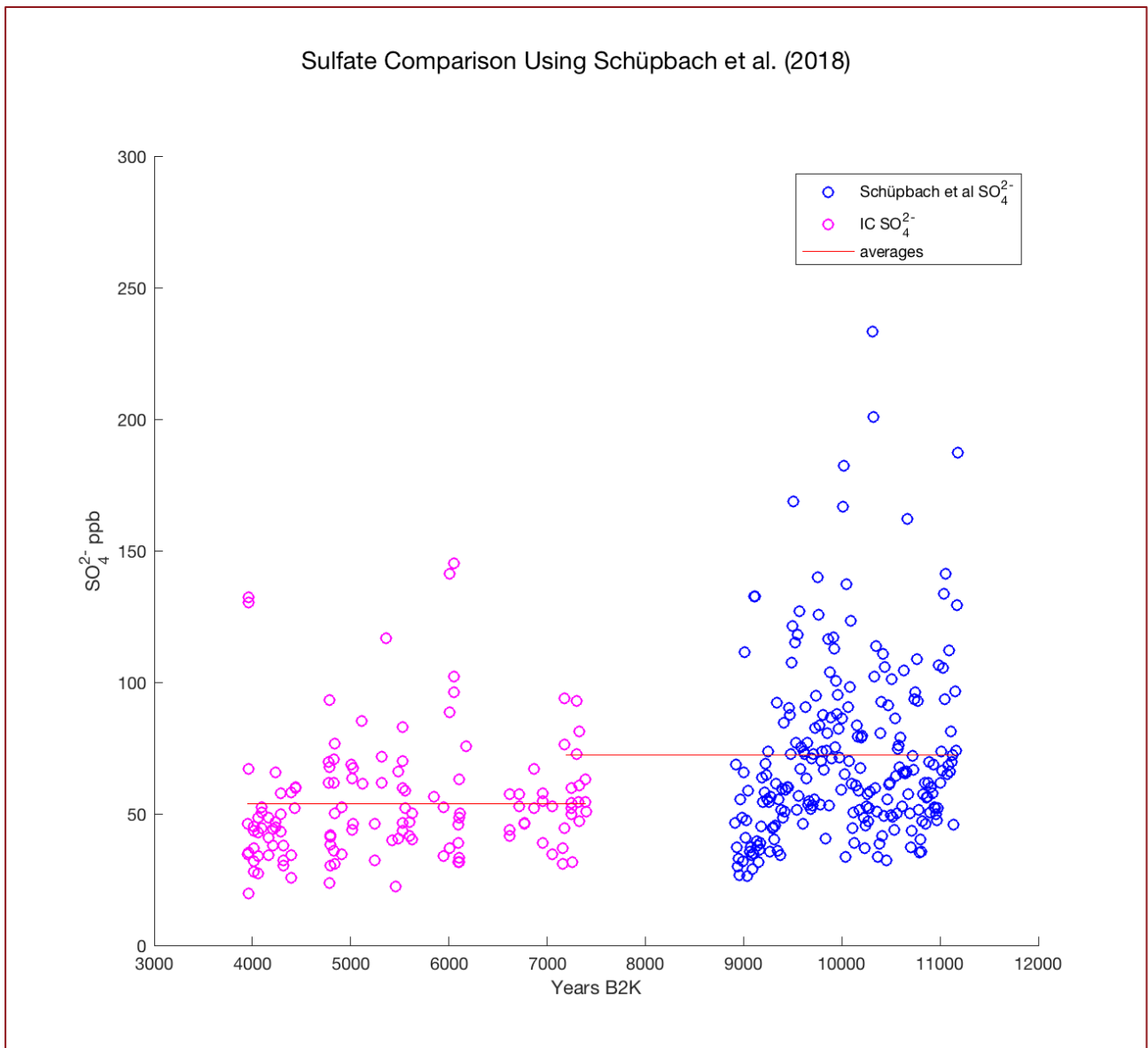


Figure 24 Comparison of IC data with that of Schüpbach et al. (2018) for sulfate.

Table 5. Table of means and standard deviations (SD) for sulfate values.

	Mean (ppb)	SD
IC data	53.7884	22.5793
Schüpbach et al (2018)	72.3261	35.5905

The published data for sulfate concentrations of NEEM begin only after 9000 years B2K and after the BZ, making direct time and depth comparison of sulfate impossible. Therefore, CFA data available after the BZ is used to compare with the IC produced values. The average IC

sulfate value and the average of the data points from Schüpbach et al. (2018) data used in this are plotted in red color. SO_4^{2-} values from CFA have values at higher extremes (Figure 24).

In order to determine if a sample SO_4^{2-} value is high enough to be categorized as potentially indicative of volcanic activity, the two standard deviations threshold is being used to define this boundary. If IC SO_4^{2-} values remain under two standard deviations from the mean in this study, then there is not enough deviation to categorize it as particularly unique.

5.5 Comparison of Br^- values

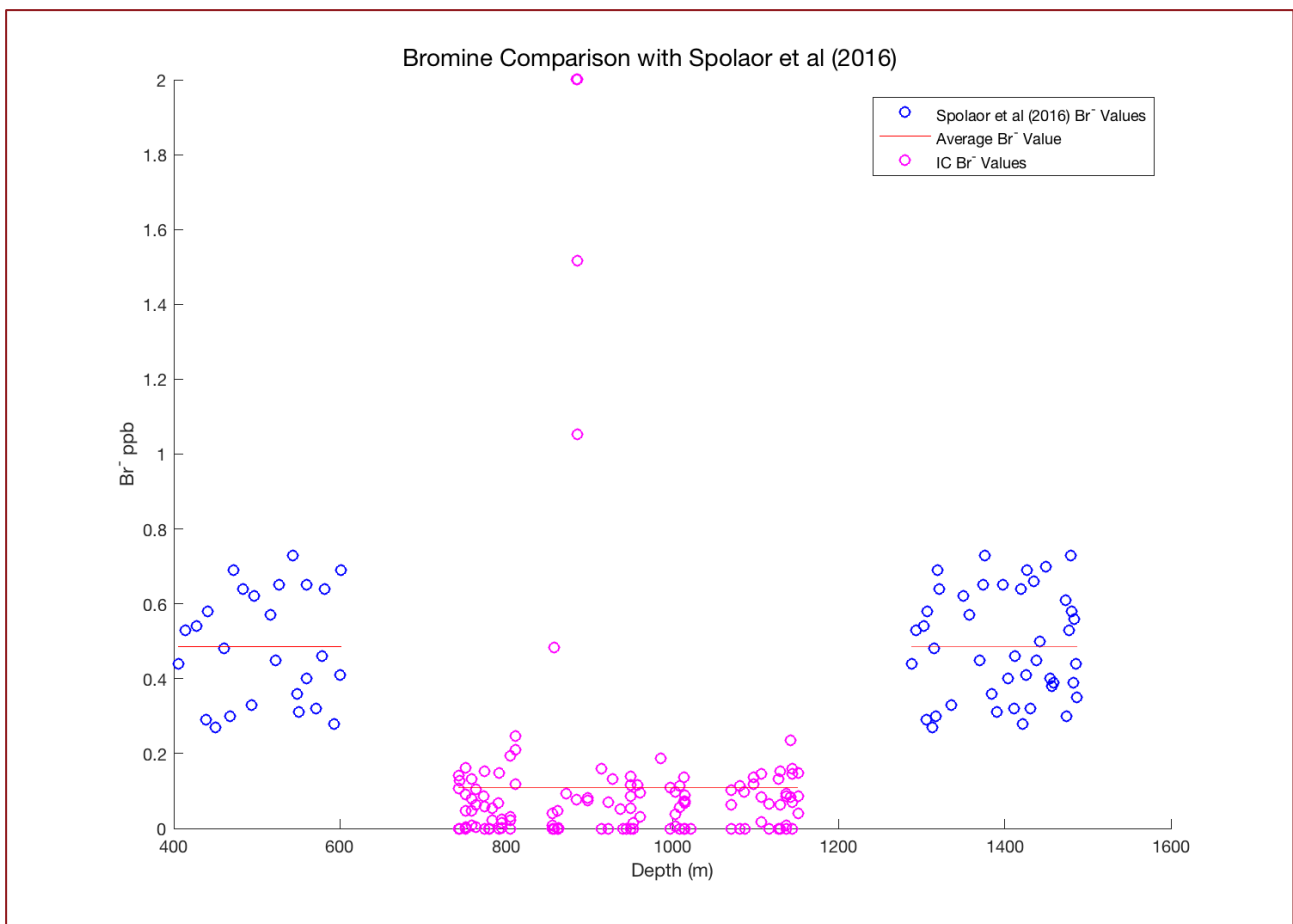


Figure 25 Comparison of IC data with that of Spolaor et al. (2016) for bromide.

The Spolaor et al. (2016) data includes bromide concentration for the NEEM ice core, but excluding the BZ. Because bromide data is not available for the section corresponding to the IC measurements, the comparison is conducted with bromide data 200 m before and after the BZ, where data is available (Figure 25). The average of each section of bromide data is shown with red lines. For the IC measurements, there are extreme outlying values in which are likely indicative of contaminated samples. These outlying values are maximized to a threshold of 2 to

reduce their influence on the mean value, but yet still remain clear outliers. Outliers are not excluded in this comparison but could potentially be done so if future analysis requires this dataset. Values under zero (negative concentration values) were set to zero. The reason for negative values may derive from the calibration and inability to discern a clear signal due to low concentrations. Potential reasons for difference in mean values between Spolaor et al. (2016) and IC data is discussed in the next chapter.

5.6 Comparison of NH_4^+ values with GISP2

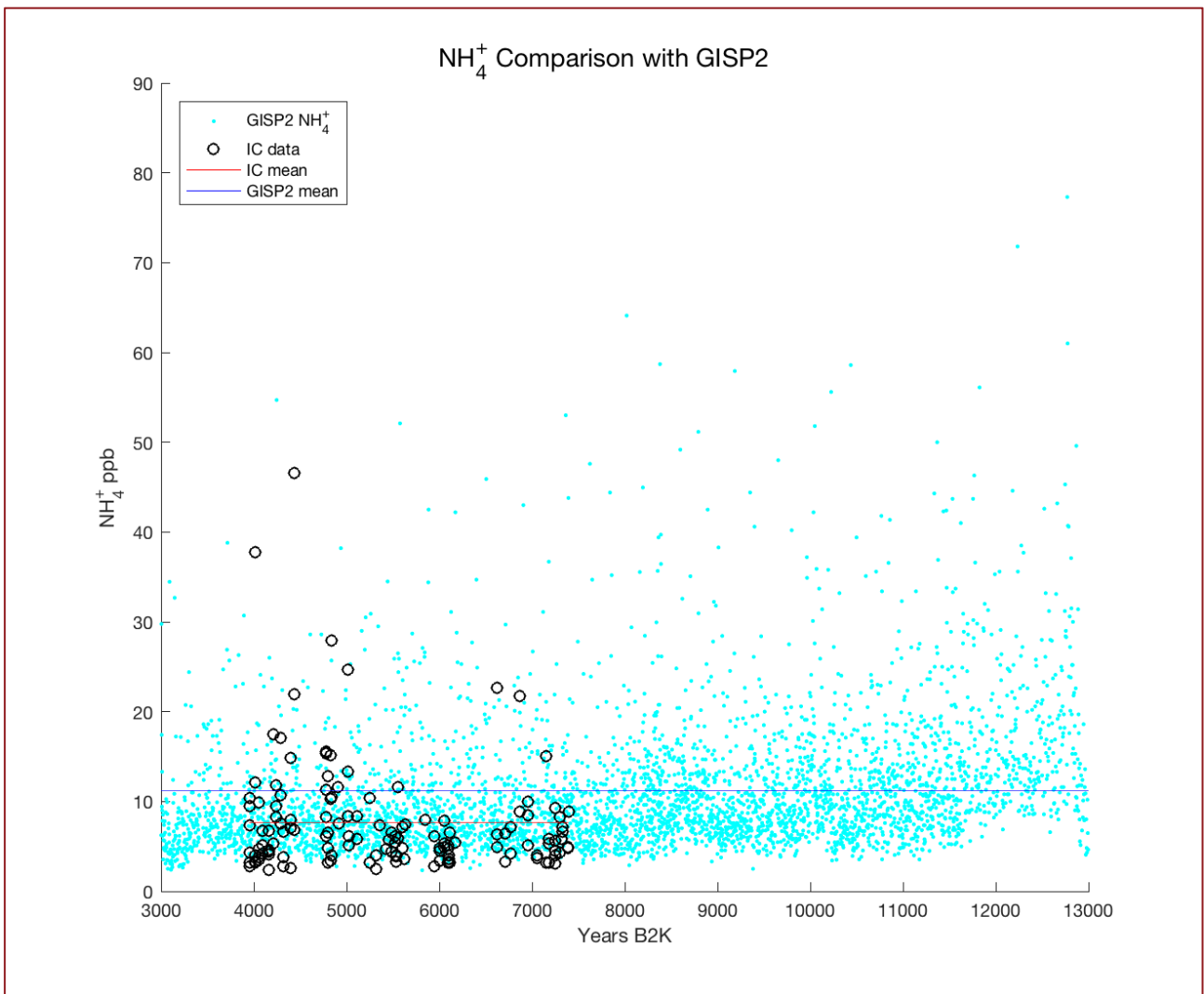


Figure 26 Comparison of IC data with GISP2 for ammonium.

The IC data for NH_4^+ is graphed in black color and the GISP NH_4^+ concentration is graphed in cyan, both with lines parallel the x-axis that indicate the mean values. The GISP NH_4^+ data derives from Fischer et al (2015) through CFA at 2-4 year resolution.

Higher values of NH_4^+ concentrations are observed at the start of the Holocene (~12,000-13,000 years B2K), reasonably so due to the relatively sudden increase of biological activity (Figure 26). These high values decrease and stabilize afterwards. The GISP 2 data shows NH_4^+ concentrations at the start of the Holocene until ~3000 years B2K and the IC data between ~4000-7000 years B2K.

Table 6. Table of means and standard deviations (SD) for NH_4^+ comparison between IC and GISP2 values.

	Mean (ppb)	SD
IC NH_4^+	7.6764	6.3010
GISP2 (~4000-7000 yr B2K)	9.5563	7.6184
GISP2 (~3000-13000 yr B2K)	11.1640	8.4845

After the large scale data set is plotted and comparison conducted, small-scale areas of interest are visually pointed out. An analysis for these areas are done below and discussed further in the following chapter. These areas of interest are distinguished by higher than average values of several ion species that together might hint to an event or particularly intense season. Events are analytically significant if concentration value(s) are two or more standard deviations above or below the mean. Conductivity is graphed with ECM or DEP (depending on which is available) to determine if the two datasets are comparable. Ions of interests for a particular depth are graphed. Together they make for hypothesis of what may have occurred at a particular time, some with relatively more certainty and evidence and others that hint inconclusively something may have happened. When put on a large scale, these events are not to the extent seen at other points in time such as glacial periods. Nonetheless, they make for an fruitful discussion of variability in the Holocene and resolution of the IC data.

5.7 Climate proxies at several depths

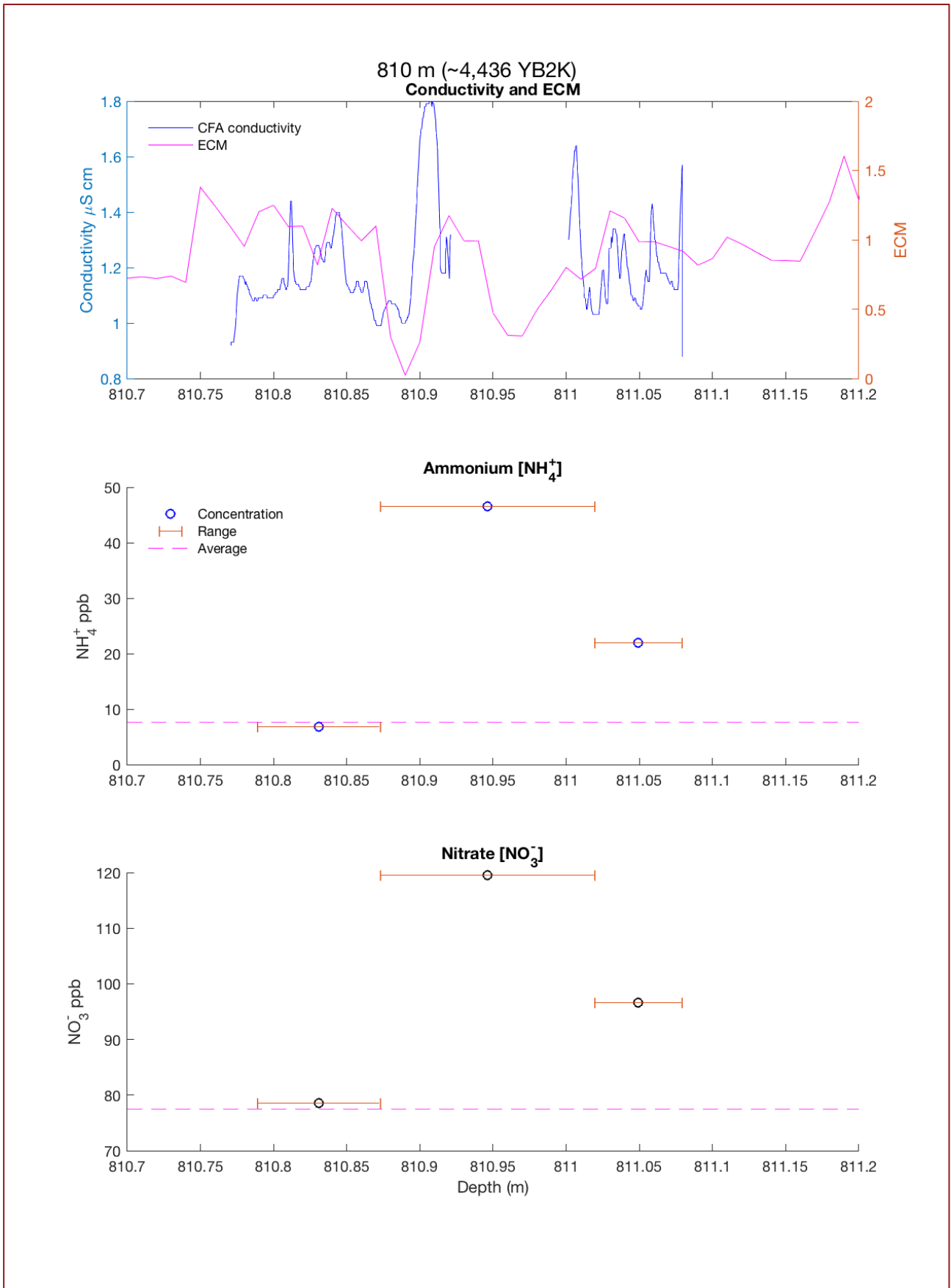


Figure 27 Analysis at 810 m where above average values of nitrate and ammonium are observed.

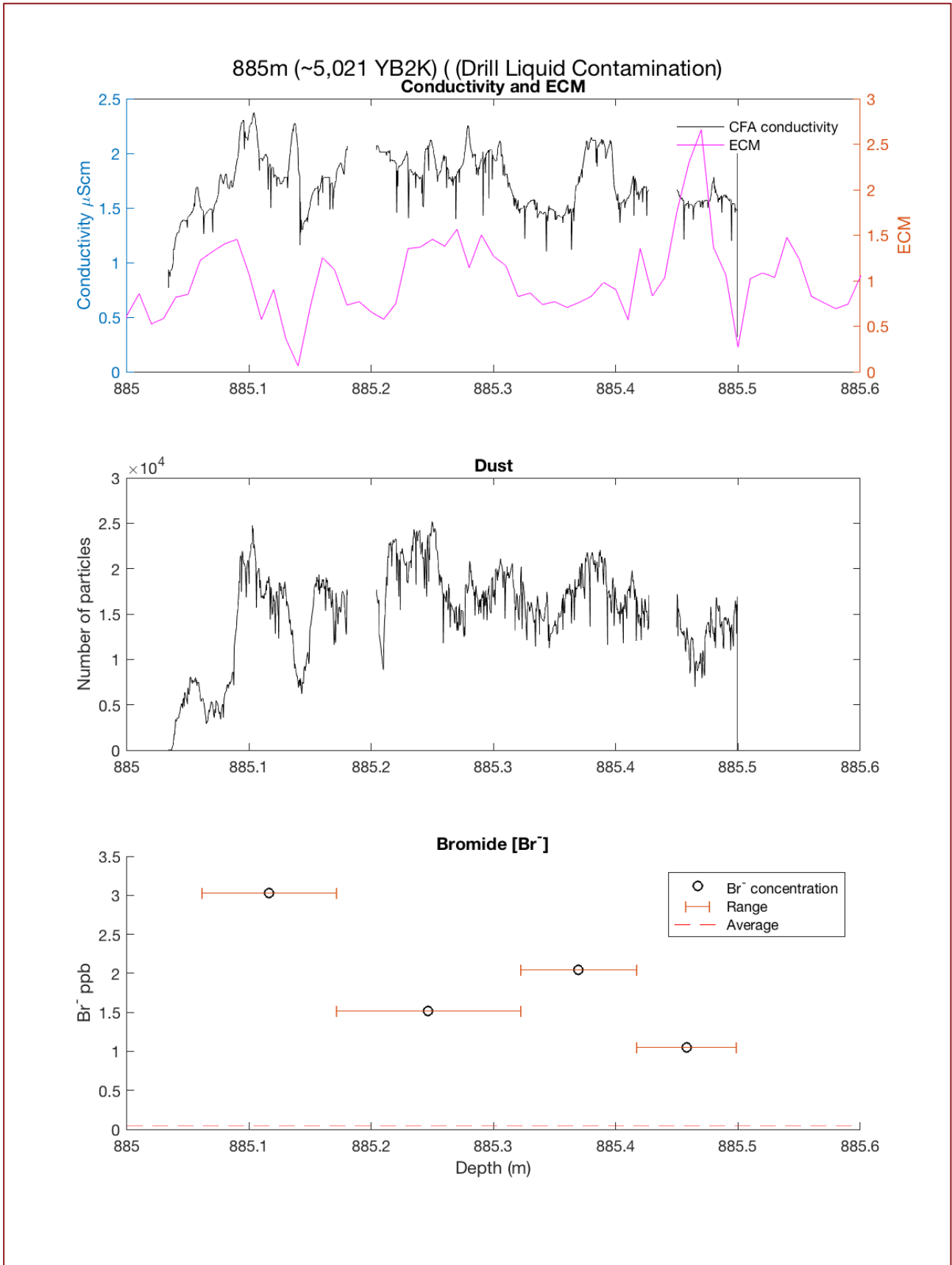


Figure 28 Analysis at 885 m, where there is evidence of drill liquid contamination coinciding with disproportionately high values of bromide. Here, no maximum threshold is placed on bromide data. In the comparison above, a threshold was placed at 2 ppb to minimize the skew in average and standard deviation calculations.

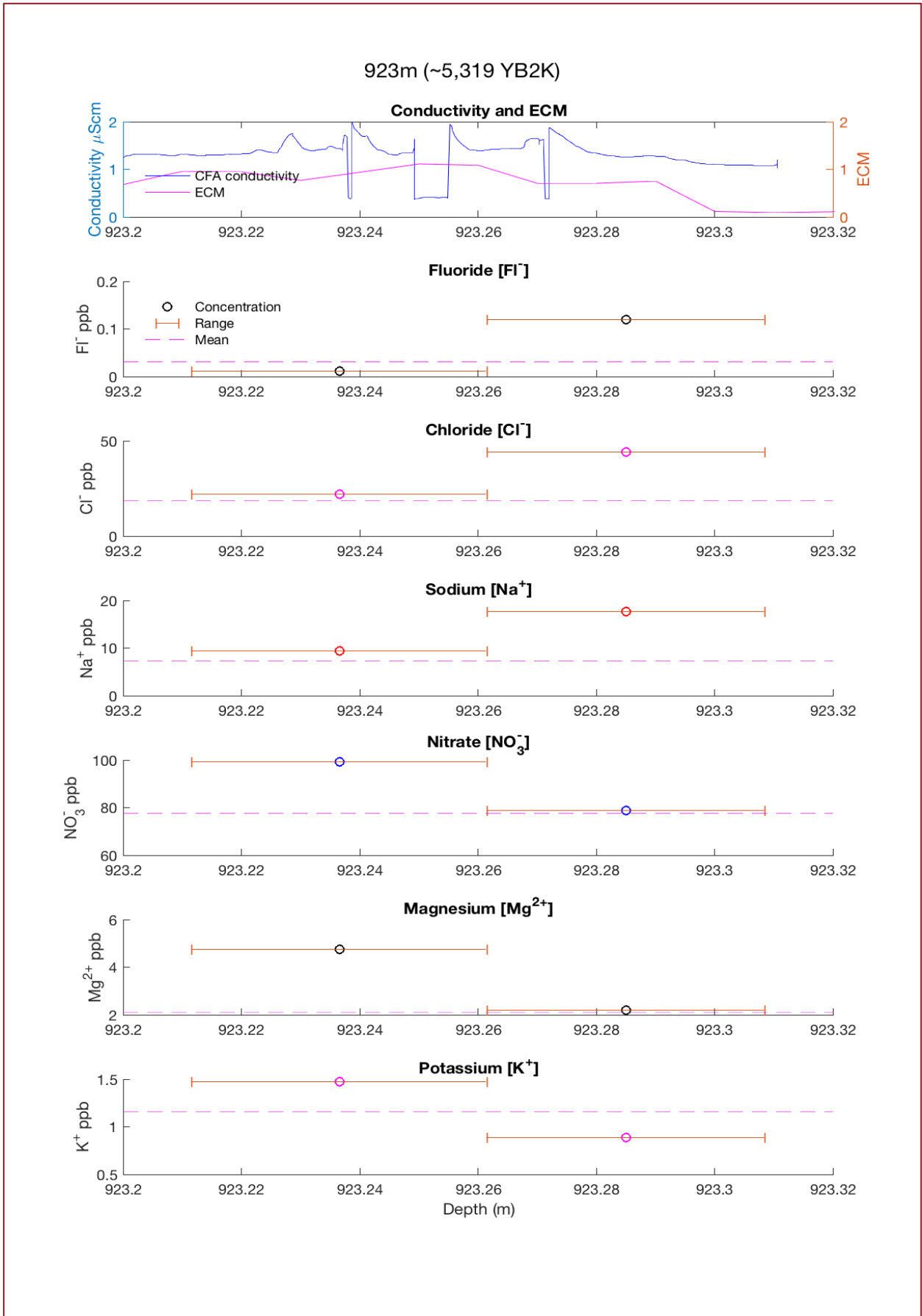


Figure 29 Analysis at 923 m, where higher sodium, chloride, fluoride, sulfate and magnesium ions are observed.

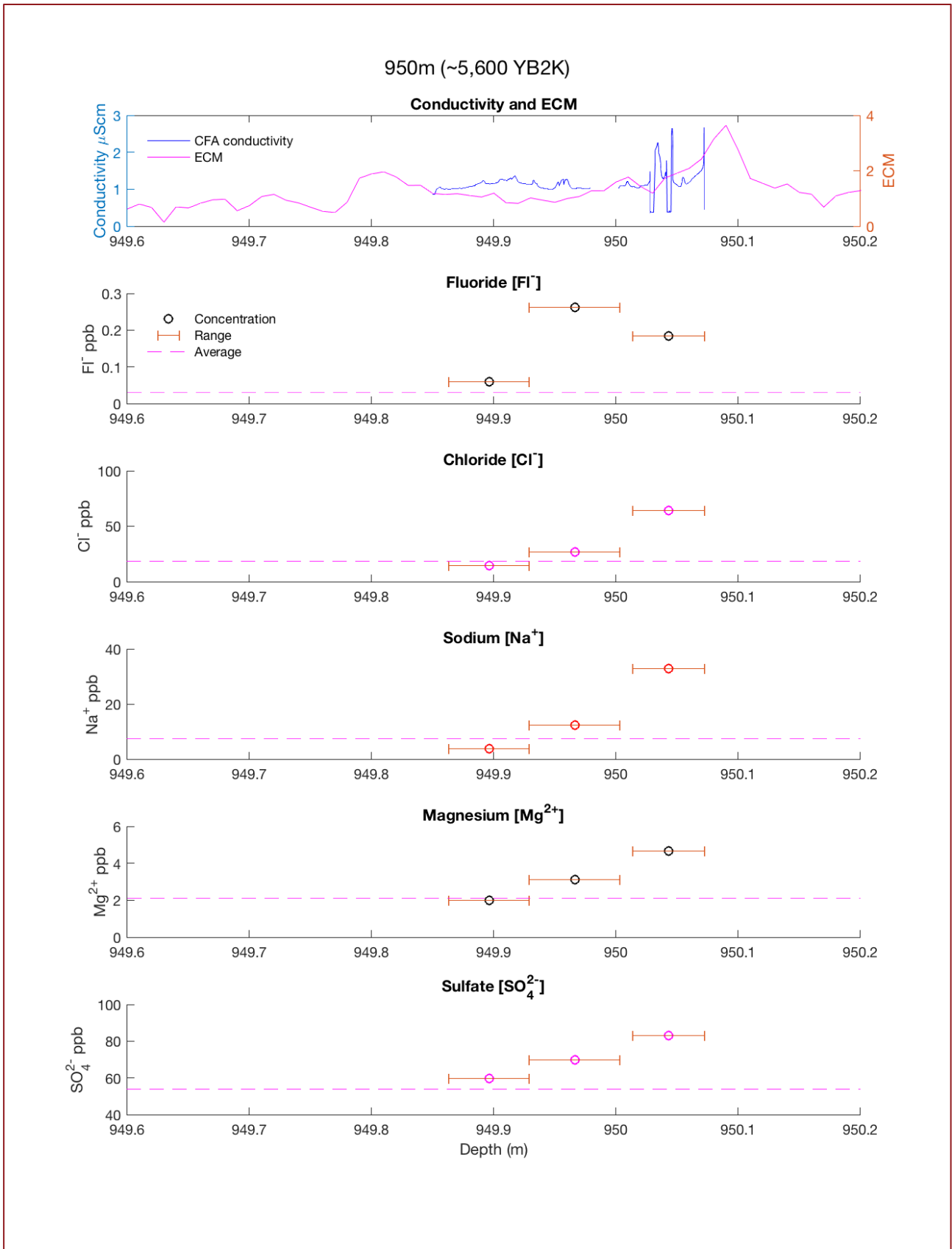


Figure 30 Analysis at 950 m where there are similar trends across several ionic concentrations.

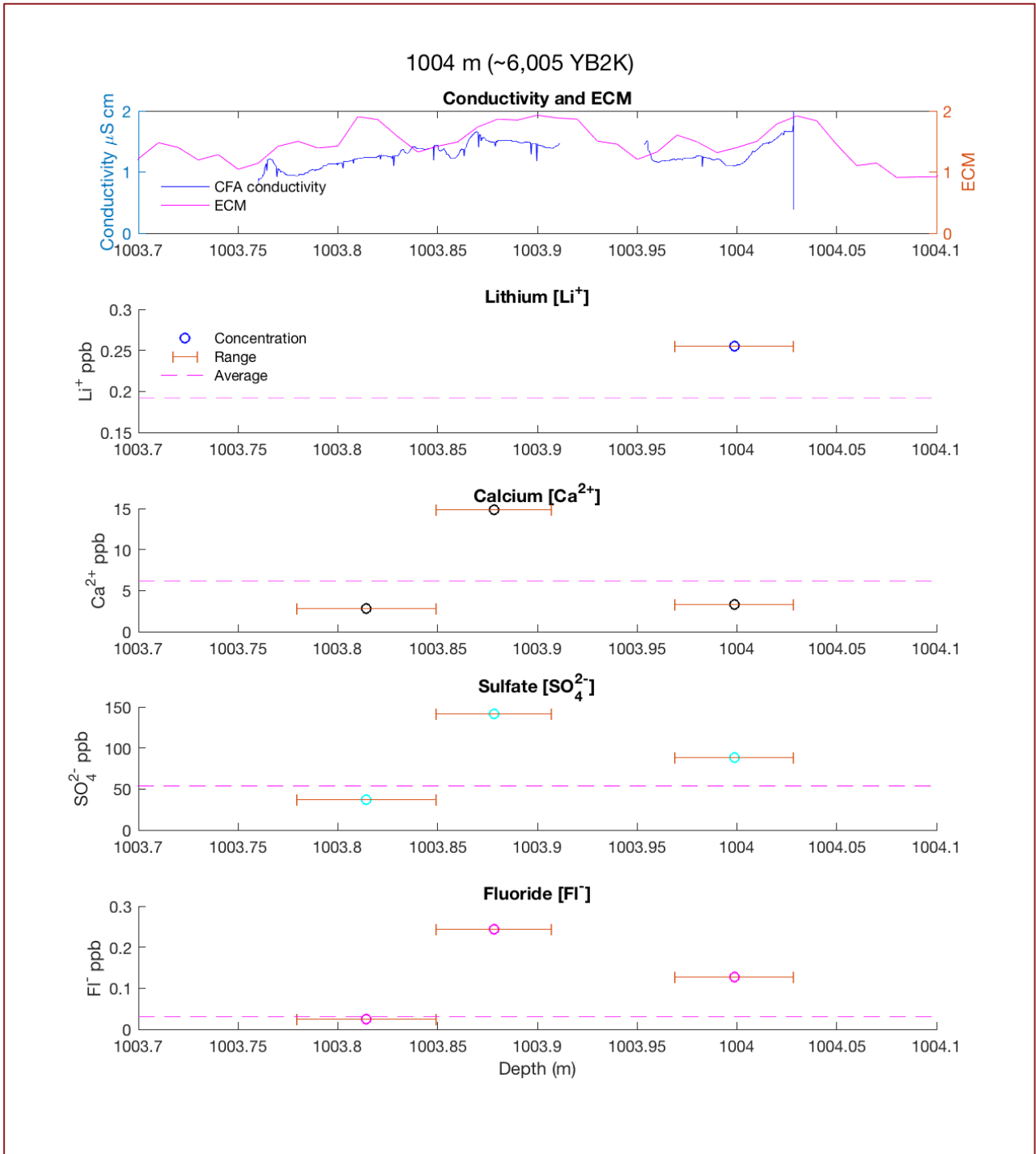


Figure 31 Analysis at 1004 m, where higher lithium, calcium, sulfate and fluoride concentrations are observed.

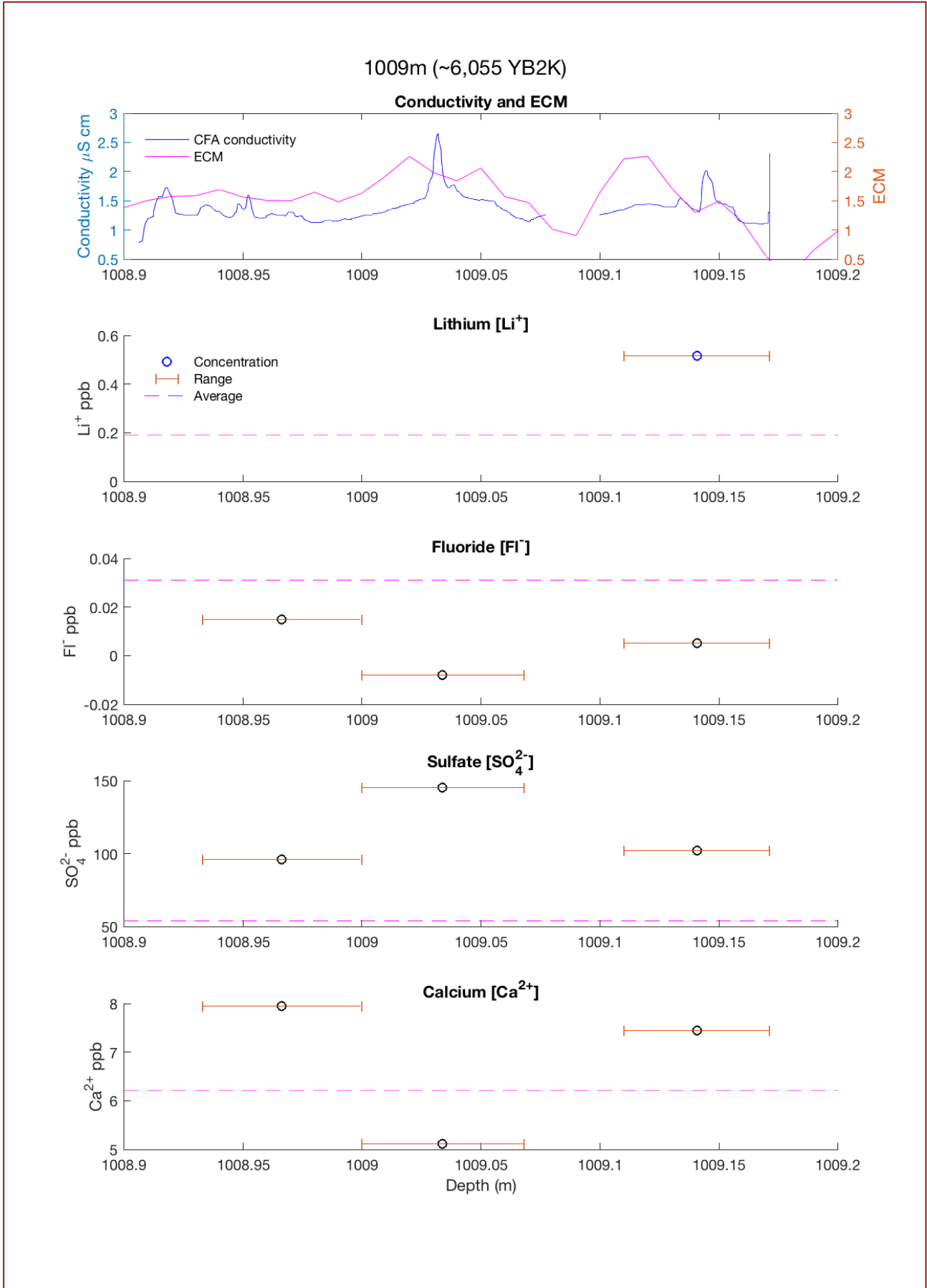


Figure 32 Analysis at 1009 m where higher lithium, sulfate and calcium concentrations are observed.

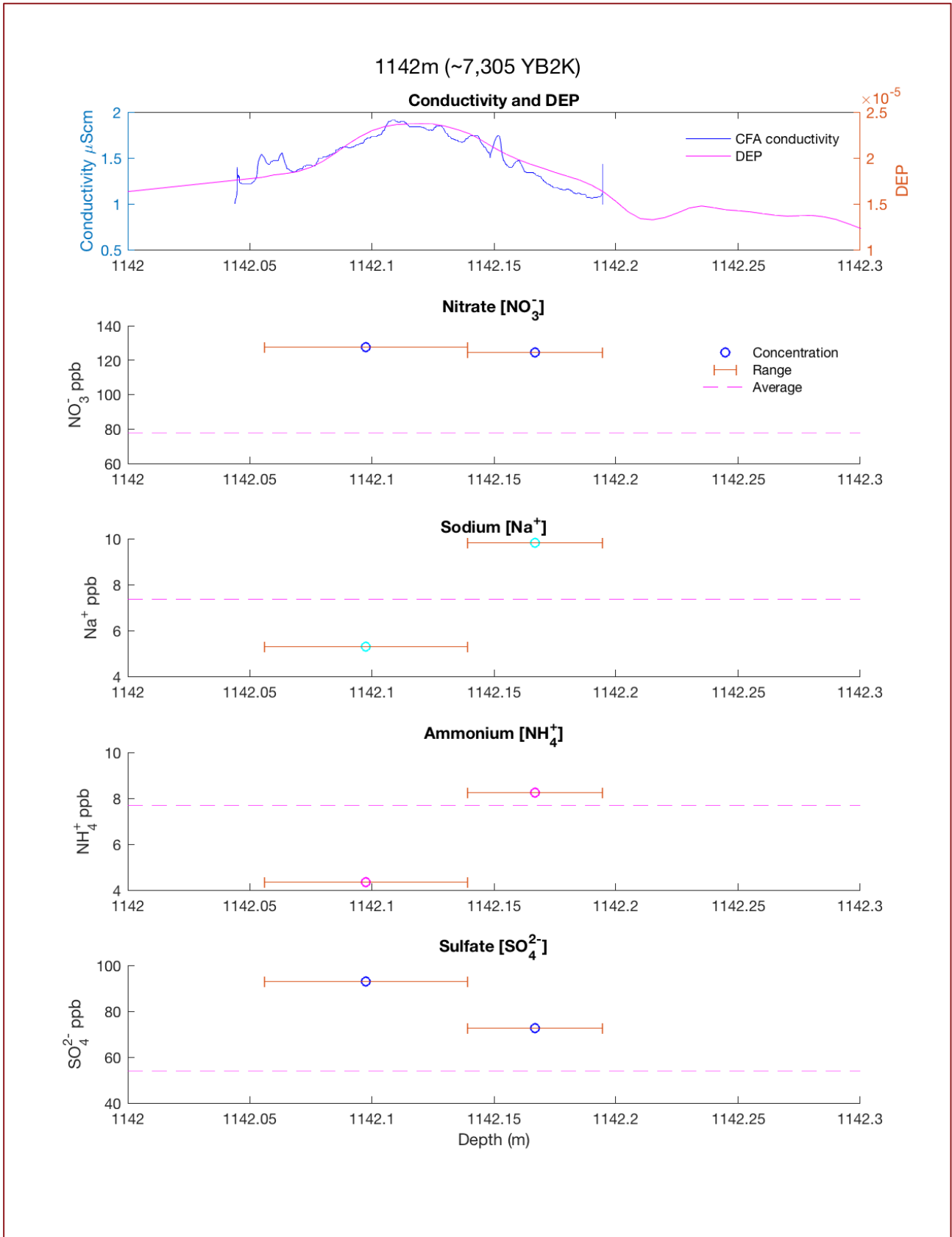


Figure 33 Analysis at 1142 m where higher sulfate, nitrate and low ammonium values are observed.

6. Discussion

The decontamination and sampling CFA method applied in this study also produced conductivity and dust data. The discrete samples were placed into the IC which measured concentrations of selected cations and anions. These concentrations were plotted with depth and time for a large scale visual, ranging from ~750-1150 m and ~4000-7200 years B2K (Figures 11-22). Because of interpolation to get time, depth was used more often for the detailed analysis in order to avoid an additional but small source of uncertainty. On the large scale, areas of interest were identified based on higher concentration values of one or more cations and anions at the same depth, which could together be a proxy for a distinct climate event. To strengthen and increase the significance of the results, comparisons were done with three other studies that had datasets that overlapped with part of the time and depth range of this dataset. Otherwise, data before and after the BZ were used for comparison. The results show that IC data is often within reasonable range and variation for the compared regions of NH_4^+ , NO_3^- , Na^+ and Ca^{2+} . SO_4^{2-} , but the published data showed more extreme values that were not seen in the IC. The IC data for bromide was deviated more from published data, however.

Despite the effort to minimize and exclude contamination, it still persisted through the disproportionately high dust peaks, often an indicator for drill liquid contamination. Drill liquid contamination was also difficult to exclude completely due to its chemical nature and seepage into large and small breaks in the ice. Contamination was also likely observed in several samples that showed irregularly high bromide values.

6.1 IC results with depth and time

In this project's attempt to fill the NEEM BZ gap of overall ice core data, the resulting figures show that concentrations remain relatively stable through the Holocene, as expected. Figures 11, 12, 13 and 14 provide a large scale look at the ionic concentrations of various species across the Holocene, previously unavailable until now. For each ionic species, the mean and standard deviation is also calculated and graphed to show the extent to which some points deviated from the average (Tables 2 and 3).

The standard deviations for the each cation and anion show that there are variations from the mean concentrations for the BZ, some ions to a greater extent than others (Tables 2 and 3). This

is illustrated by the high SD value relative to the mean. However, the bromide mean and SD data may not provide a true representation due to contamination present in some values that distort the statistical calculations despite placing a maximum threshold for bromide concentrations at 2 ppb, which is still much higher than the mean. From the means and SD, it can be inferred that the Holocene period, known to be relatively stable, still had variability and that variability observed from IC values are likely true values.

This is not the case for ions that typically have low concentration values, such as bromide. Bromide has proven unreliable here. For a clearer perspective on bromide, the suspected contaminated samples can be eliminated and the statistics calculated again. True values for fluoride are likely, despite high variability, but with no clear indication of contamination. However, this study is not able to verify the fluoride data by comparing IC values to already published data of coinciding depths or depths of close proximity before and after the BZ.

Sea ice (Br⁻)

The concentrations of bromide remained low for most samples, with an average of 0.04 ppb including all samples and with outliers at 885 m (Figures 12 and 14). However, it is likely that these outliers derive from contaminated samples (high dust concentrations were also observed) and are therefore not representative of the dataset. Negative values also reduce the reliability of Br data. Bromide is a proxy for FYSI and the relatively higher values signify FYSI. Generally, Br values decline inland due to deposition and depletion. In this study, there is not enough signal or continuity in data to discern a seasonal cycle of bromide that indicates FYSI.

Sea salt (Na⁺, Cl⁻, K⁺ and Mg²⁺)

The presence of sea salt in ice on the Greenland ice sheet can be a proxy for wind intensity. With higher presence of these ions, it can be inferred that winds and sea ice conditions were greater. Na⁺, Cl⁻ and Mg²⁺ have visually similar trends (Figures 11, 12, 13 and 14). However, K⁺, also a sea salt ion, does not follow the same trend as closely relative to the other sea salt ions. This may be due to the sources of K⁺ and Mg²⁺, as their primary sources derive from mineral dust rather than sea salt. While Ca²⁺ is part of sea salt and sea water, it is not expected to be significant enough to serve as a primary proxy for sea salt.

A calculation to determine the amount of sea salt and non-sea salt components of IC concentrations of species that are present in seawater are presented below. An assumption is

made that average Na⁺ concentration from the IC is accurately representative of sea salt. Na⁺ is used as the basis for non-sea salt(nSs) calculation for subsequent ions as Na⁺ is a clearer proxy than Cl⁻ for sea salt, as Cl⁻ may have other sources such as volcanos.

Table 7. Sea salt and non-sea salt (nSs) components of various ions that are known to be present in seawater.*

Sea Salt Ion	IC Concentration (ppb)	Average Non-seasalt Component (ppb)	(nSs) Percentage as Sea Salt
Na ⁺	7.3529	0 (<i>assumption</i>)	100% (<i>assumption</i>)
Cl ⁻	18.4847	5.2935	71.36%
Mg ²⁺	2.1185	1.2249	42.18%
Ca ²⁺	6.2047	5.9650	3.86%
K ⁺	1.1607	0.8885	23.45%

*Detailed calculations are presented in the Appendix A.

The assumption made was that all Na⁺ concentrations measured on the IC are from seawater and that all Na⁺ in sea salt was accounted for. Based on this assumption, 71.36% of the measured IC concentration of Cl⁻ derive from seawater and sea salt and the remainder from other sources, possibly volcanic HCl, for example (Table 7). Only 3.86% of Ca²⁺ present in samples is from sea salt, which is reasonable as Ca²⁺ is mostly a proxy used for mineral dust and not expected to constitute much of sea salt. Mg²⁺ constitutes a larger portion of sea salt than K⁺, which may be used to hypothesize why Mg²⁺ concentrations seen Figures 12 and 14 are visually more similar to Na⁺ and Cl⁻ than K⁺ is.

Volcanos (SO₄²⁻, F⁻ and Li⁺)

A maximum value of 145 ppb of SO₄²⁻ is observed in the IC concentrations (Figures 12 and 14). Due to dilution of sample in a tube, the actual concentration may be higher. Overall, volcanic activity during the measured time period of the BZ do not reach the extent seen in other periods. For example, the Tambora volcanic eruption of 1815 A.D yielded about 350 ppb of sulfate in the Summit (Greenland) ice core, which is more than double of what is observed in the max IC concentrations of SO₄²⁻ for NEEM BZ (Cole-Dai, et al., 2009). It is possible that Icelandic volcanic activity is detected in sulfate here, as there are instances of increased sulfate, lithium, and fluoride concentrations but with no indication of large volcanic activity.

Forest fires (NH₄⁺)

The highest value of NH₄⁺ observed is at 45.6 ppb, which may indicate the potential for a summer season and record of wildfire (Figures 11 and 13). While NO₃⁻ can serve as another proxy for biomass, no visual relationship or trend can be determined between the two ions where there are above average values of one or the other. A further look into IC NH₄⁺ values relative to the rest of the Holocene period from published data will be presented in the following subchapters.

Atmospheric nitrogen, temperature and accumulation (NO₃⁻)

Nitrate values have an average of 77.51 ppb, with many values both above and below the average, demonstrating that there few outliers in the data and the mean is representative of the true values (Figure 12 and 14) (Table 3). In measurements of lower NO₃⁻ concentration, it can be hypothesized that temperature was cooler and accumulation was lower, but with considerations regarding evaporation and photolysis of NO₃⁻ on the surface. While values here are considered true signals, there are not enough sampling points to see clear annual cycles and to see them consecutively. Potentially, part of or one annual cycle can be seen in the data at some depths, which can help indicate a season.

Mineral dust (Ca²⁺, Mg²⁺, K⁺ and Li⁺)

Relative to Mg²⁺ and Li⁺, Ca²⁺ does not visually have large outliers in the data and concentrations remained relatively stable with a mean of 6.21 ppb (Figures 11 and 13) (Table 2). Mg²⁺ and Li⁺ are also proxies for other events, such as salt and volcanic activity, while Ca²⁺ is largely indicative of dust. Dust in the Holocene is generally much lower than that observed during glacial periods. In the LGM, Ca²⁺ concentrations were generally much greater than 100 ppb. The Ca²⁺ values observed here are comparable to that observed in the Eemian period, which is reasonable as it was also a warmer interglacial period (Schüpbach et al., 2018). No analysis has been done to determine if there is any statistical relationship between these dust proxy ions.

The method carried out in this study begins to unravel the BZ, in which there was little to no previous chemistry data available for in the NEEM ice core. Here, we can see that on a large scale, spanning between 3900 and 7300 years B2K, there is relative stability. This matches the data provided by the stable water isotopes. Changes on a small scale overtime cannot be detected well through this method, as many samples are still excluded and the overall

fragmentation and sampling of the dataset does not provide enough resolution. This poses a challenge to discern if there are seasonal cycles consecutively or if there are changes and trends happening on a decadal or centennial scale.

However, some instances in which several ions show above average values at the same depth and time can be interpreted for potential climate events or higher intensity seasons. It is important to note that calibrations may affect the results to a greater extent for ions that inherently have low concentrations and signals, such as fluoride and bromide. However, this applies less so to ions in which are more frequently present in ice cores.

6.2 Comparison with Schüpbach et al. (2018) for NH_4^+ , NO_3^- , Ca^{2+} and Mg^{2+}

The data produced cannot be directly verified and hence, the dataset from Schüpbach et al. (2018) is used in order to get a sense of where the IC data lie respectively. However, the IC data could not be compared as a whole because the Schüpbach et al. (2018) dataset only begins after the BZ ends with only an overlap of about 250 m of data. The comparison is drawn between Schüpbach et al. (2018) and the IC produced data, with the average of comparable ions from Schüpbach et al. (2018) shown on the IC data. 19 values from the IC can be compared with Schüpbach et al. (2018) (Figure 23).

Table 4 shows the averages and standard deviations of the dataset used in this comparison. Na^+ and Ca^{2+} both had higher averages from the Schüpbach et al. (2018) data compared to the IC data. Schüpbach et al. (2018) show 11.41 and 6.73 ppb for Na^+ and Ca^{2+} whereas the IC data yield 5.84 and 4.38 ppb. Both had very similar standard deviations. NH_4^+ and NO_3^- concentrations were generally lower in the Schüpbach et al. (2018) data than in the IC produced data, with concentrations at 4.35 and 76.68 ppb for NH_4^+ and NO_3^- in the published data in comparison to 6.09 and 78.71 ppb otherwise. Standard deviations were similar for NH_4^+ but differed more for NO_3^- , with 14.84 from Schüpbach et al. (2018) and 20.82 from the IC.

It is unclear what could be causes of variability for the means between the two datasets, particularly for Na^+ . Across the four compared ionic species, variability between means can be influenced by dilution and sampling method. The published dataset was produced from CFA procedure, whereas the IC used discrete measurements. CFA data is presented as an average of 10 years whereas the IC data includes sample at an annual scale, but fragmented in depth and time. The discrete measurements create a sample of meltwater diluted over the period of

collection. For example, if a forest fire occurred with high NH_4^+ values, the discrete IC sample would include the meltwater deriving from the forest fire as well as meltwater corresponding to the time before and/or after, creating an average and diluting the true NH_4^+ value of the forest fire. If this is the instance, a continuous method would be capable of distinguishing this particular event from the surrounding baseline, potentially creating higher values and peaks than seen in the IC data, but averaged over 10-year periods. Furthermore, CFA is quick and only captures the most soluble portions of ions, whereas ions (such as sea salt) have more time to dissolve in IC samples that have been frozen and melted again over a longer period.

6.3 Comparison with Schüpbach et al. (2018) for SO_4^{2-}

SO_4^{2-} data is from Schüpbach et al. (2018) and is only available for depths after the BZ. While a direct comparison of time and age cannot be done, there is still valuable information gained by comparison of the two datasets, both of which are still in the Holocene period. The IC SO_4^{2-} values have a mean of 53.23 ppb and a standard deviation of 22.58 compared to 72.33 ppb and 35.59 from the Schüpbach et al (2018) area depicted (Figure 24) (Table 5).

There are more extreme sulfate values observed in the published dataset than compared to the IC (Figure 24). At most, IC SO_4^{2-} concentrations reached about 145 ppb, compared to 233.2 ppb. The averages calculated are affected by these high values (Table 5).

The IC data produced contain resolution of about half year in one sample, given that the accumulation rate is about 11 cm/year at BZ depth. Schüpbach et al. (2018) data is provided as 10-year averages, which arguably also creates a dilution effect that smooths the overall extreme values of sulfate samples. The produced IC data still did not yield SO_4^{2-} values as high as that of Schüpbach et al. (2018), which either is indicative of relative less volcanic activity or that sample fragmentation has excluded data that may have otherwise contained data for volcanic activity.

6.4 Comparison with Spolaor et al. (2016) for bromine

The data from Spolaor et al. (2016) excludes values for the BZ. Therefore, data before and after the BZ are used to compare the bromide IC concentrations (Figure 25). The Spolaor et al. (2016) values average around 0.5 ppb whereas the average Br concentration from the IC is about 0.04 ppb. While the contaminated data was not excluded in order to remain transparent, the limits were put in place at 2 ppb in order to minimize the outliers and their influence on the mean.

Negative values were set to zero. Nonetheless, the means remain much lower with data from the IC.

One reason that constitutes this difference is due to the method of measurement. Bromide data from Spolaor et al. (2016) derives from Inductively Coupled Plasma Mass Spectrometry (ICP-MS) where sample is injected with hot plasma in which electrons are removed and ionization occurs. The ion of interest is separated from its surrounding polyatomic species. Mass-to-charge ratio is used to separate the ions of interest as they remain stable enough to pass through the quadrupole. ICPMS is able to analyze traces over a wide range. However, it does not distinguish between the different types of bromine and results in data that consists of all bromine and hence, higher concentration values. The use of the IC targets Br^- only. Even with the use of the IC, only soluble Br^- is analyzed and insoluble Br^- remains undetected, however.

6.5 Comparison with GISP2 for NH_4^+

The use of GISP2 data provides a comparison not only from a different dataset, but also from a different ice core and location. NH_4^+ is used for comparison between IC values and GISP2, as it is a climate proxy that is relatively better understood. GISP2 data covers the entire Holocene to give a large scale visual of how the IC data fits. The GISP2 NH_4^+ shows greater extreme values than the IC because the GISP2 data derives from CFA at 2-4 year resolution and with less fragmentation. The IC data may have missed some of the higher peaks in NH_4^+ concentration due to sample dilution as well as data fragmentation (Figure 26).

More extreme NH_4^+ values are observed at the start of the Holocene, around 13000 years B2K which is consistent with the burst in biological activity at the same time due to warmer climate (Figure 26). Over the course of the following several thousand years, NH_4^+ concentration declines and stabilizes. At the time in which the IC values and GISP2 data overlap, NH_4^+ values look relatively stabilized and do not visually look as if they are continually decreasing. Peaks in the IC values are not as extreme as that observed by CFA in GISP2.

The period of GISP2 NH_4^+ data (3000-13000 years B2K) used has a mean value of 11.16 ppb and a standard deviation of 8.49 whereas the IC NH_4^+ data has a mean of 7.68 ppb and standard deviation of 6.30 (Table 6). The standard deviation proves difficult for differentiation as the two datasets do not have the same number of samples and therefore, variability between the two cannot be compared. Mean values for the GISP2 dataset is higher and this is likely so due to the

inclusion of the higher peaks visible at the start of the Holocene. Furthermore, the GISP2 data has more continuous and has the ability to detect more events and seasons. If only the period of 3500-8000 years B2K is considered in GISP2, the mean is 9.66 ppb, which is quite comparable to the IC NH_4^+ average (7.68 ppb) (Table 6).

The averages demonstrate that IC values are about 1.98 ppb less than the GISP2 values at approximately the same time span. When compared to the mean of the entire Holocene of GISP2, the IC average is 3.49 ppb less (Table 6). In both instances, the IC average lies below that of GISP2, potentially due to sampling methods.

6.6 Special Cases for Analysis

While the data on the large scale showed a trend of relative stability, an investigation into the details lend insight into variability and a discussion of how well the IC method used in the BZ can distinguish climate events through proxies. The large scale visualization of the IC data does not sufficiently show the extent of the fragmentation of data due to ice quality and too few samples. Higher concentrations of specific cations and anions seen in Figures 11-14 lead to a small scale analysis of a possible event (i.e volcano and forest fires) based on climate proxies. Concentrations are considered significant if they were two or more standard deviations above mean value. If discrete measurements are able to distinguish events within reasonable uncertainty, then NEEM BZ can further be able to be sampled using the method applied here and therefore, can provide data that can be used to further elucidate the Holocene period.

810 m (Bag 1475)

A break in the ice occurred during the collection of the sample, in which coincides with high ammonium and nitrate values at 810.95 m. The NH_4^+ value at the peak is more than four standard deviations from the mean value (Figure 27). NO_3^- value at the peak is greater than two standard deviations from the mean value. Both ions show a significant variability beyond the normal (one standard deviation) values, leading to two hypotheses. One could be that contamination at the breaks occurred and was collected in the sample tested on the IC. Often, human contamination from ice processing is evident as high ammonium values. Another is that an event, such as a wildlife, may have occurred. These two ionic species serve as proxies for ecological activity, vegetation growth and wildfires. Furthermore, the relatively higher values of NO_3^- tend to indicate warmer temperatures, which could reasonably fit with and support the hypothesis of Northern Hemisphere summer wildfires and biological activity.

885 m (Bag 1610)

An indication of contamination can be seen in the dust concentrations of Figure 28. The levels remain consistently high with no clear signal indicating true values. Furthermore, conductivity remains consistently higher than ECM, demonstrating an altered baseline. The source of contamination is likely due to the presence of drill liquid. Prior to melting, cracks were observed along section of ice. With the knowledge of the likeliness of contamination, this section of ice was melted at the end of all CFA experiments with the scientific intention to explore the impacts of drill liquid on resulting dust and IC measurements.

While the presence of drill liquid is confirmed, there is, coincidentally, usually high amounts of bromide detected. Estisol 240 and Coasol are known to be esters, particularly di-isobutyl esters, with no clear evidence of bromide applied. No relationship at this time can be discerned between drill liquid and bromide and no other samples share this characteristic of uniquely high dust and Br. Nonetheless, the effects of drill liquid are clearly shown in dust measurements, but not so much in chemistry.

923 m (Bag 1679)

The conductivity shows periods of interrupted sampling and melting with no clear trends, proving unreliable for analytical use (Figure 29). Na^+ , Cl^- and F^- share similar trends at this depth. Na^+ concentration (17.64 ppb) is almost two standard deviations higher than average whereas Cl^- concentration (44.08 ppb) is more than two standard deviations higher. Mg^{2+} , K^+

and NO_3^- are at average where Na^+ and Cl^- are high, but increases to a two standard deviation extent afterwards. With high values in sea salt ion, it can be inferred that it was the winter season.

K^+ and Mg^{2+} show higher values after the sea salt ions have peaked, indicating a possible increase in dust that could potentially be observed at the start of spring (Figure 29). NO_3^- peaks also indicates a warmer period of an annual cycle. While an above average F^- value was singled out, it is difficult to determine the source and if there is any significance, as F^- concentrations are often associated with volcanic activity and acidity, rather than sea salt, wind, temperature and accumulation. The chemistry data here supports the presence of an annual cycle from winter to spring and is even more evident with ECM data present.

950 m (Bag 1728)

The conductivity produced through CFA sampling here also exemplifies instances in which melting was interrupted (Figure 30). Where there are true values for conductivity, they fall in the range of ECM data, but the possible peak at 950.1 m was perhaps missed. SO_4^{2-} concentration at 950 m is about one standard deviation from the mean of the at 83.07 ppb and does not signify a particularly high value that could be indicative of volcanic activity. However, F^- values are more than two standard deviations greater than average. Both Na^+ and Cl^- concentrations are greater than two standard deviations above the mean (Figure 30).

From this it can be inferred that there was a relatively higher concentration of sea salt in ice at this point, which can derive a cold season and from increased windspeeds that carry sea salt from the coastal regions inland and deposited at NEEM. In this case, higher Mg^{2+} could potentially be due to the presence of sea salt, rather than dust. Dust peaks in the spring, but sea salt ions here indicate that a cooler season is more likely. The high presence of F^- can be indicative of volcanic activity, which can be confirmed by the peak in ECM data. However, SO_4^{2-} values are above average but not outstandingly high. The conductivity peak does not warrant any large volcano occurred per se, but just perhaps that volcanic activity was present at the time.

1004 m (Bag 1826)

The trends in conductivity and ECM are comparable (Figure 31). The Li^+ value (0.255 ppb) is less than one standard deviation from the mean. There is not value before or after to compare or to indicate a trend, as Li^+ is a proxy for both volcanic activity and dust. Ca^{2+} value at its highest

peak here (~1003.9 m) is 14.86 ppb, which is more than two standard deviations from the mean. SO_4^{2-} and F^- values are both well above average at 141.2 and 0.243 ppb, which are three and two standard deviations from the mean at 1003.9 m. Peaks in Ca^{2+} , SO_4^{2-} and F^- coincide at the same depth. The conductivity reaches about 2 $\mu\text{S}/\text{cm}$ at the highest, but with no clear indication of volcanic activity (Figure 31). However, SO_4^{2-} and F^- ionic concentrations suggest that there could be potential for volcanic activity. Otherwise, SO_4^{2-} may be explained by dust carrying high sulfate content. The evidence in this respect remains unclear, but dustier conditions are also plausible as indicated by higher values of Ca^{2+} and Li^+ .

1009 m (Bag 1835)

The conductivity and ECM data show similar trends, but the conductivity has a distinct peak at ~1009.03 m (Figure 32). The Li^+ concentration is more than two standard deviations from the mean, but there are not enough values before or after to indicate a trend of increasing or decreasing Li^+ . Ca^{2+} has above average concentrations at 1009.15 and 1008.95 m, but remain less than one standard deviation from the mean, indicating that there may not be enough significance in these values that can be evidence for dustier conditions.

Sulfate values are about two standard deviations from the mean in the same sample that Li^+ yielded higher values. At the SO_4^{2-} peak (~1009.04 m), SO_4^{2-} values are more than three standard deviations from the mean. Based on the calculated mean values, the variability here can be demonstrative of the presence of volcanic activity, as these values deviate significantly from other observed values at this period (Figure 32). The presence of the high Li^+ value adds to this theory, but F^- concentrations undermine it. For the purpose of cross-comparison, the SO_4^{2-} value at the peak (1009.4 m) is two standard deviations from the Schüpbach et al (2018) values for mean and standard deviation.

1142 m (Bag 2077)

Conductivity and DEP data show a close relationship for the sampling period at 1142 m (Figure 33). There are high nitrate values of about 127.5 and 124.7 ppb respectively, both of which are more than two standard deviations from the mean. Na^+ values are not greater than one standard deviation, which is not enough to indicate a sea salt event. The high presence NO_3^- demonstrates potential for a warmer season and higher accumulation rates. However, NH_4^+ values at 1142.17 m do not indicate the presence of ecological activity.

There is, however, a decrease in NH_4^+ values at 1142.09 m that coincides with an increase of SO_4^{2-} values at the same depth. SO_4^{2-} values reach 92.81 ppb, which is slightly less than two standard deviations from the mean. This coincidence may be evidence for the reaction of SO_4^{2-} that overcomes and dominates that of NH_4^+ , a chemical reaction often observed with volcanic activity (Figure 33). While the peak is not particularly large or distinct, chemistry data supports the evidence of potential volcanic activity.

Based on the small scale analysis at various depths, conductivity data was helpful when there were no interruptions in melting to match with ECM or DEP for seasonal cycles or indicators of volcanic activity. These above cases for analysis examined how various ions are related to one another and how together, they can become evidence for wind, temperature, accumulation, biomass burning and volcanic activity. While on the large scale, the Holocene was relatively stable, the small scale comparison at various depths demonstrate regular variability.

There were cases in which an events, such as volcanoes in 1009 and 1142 m, were able to be detected from the background with reasonably more evidence. However, other instances, such as that observed at 950 and 1004 m, were unclear. The IC method help create some clarity in the BZ on a small-scale, but still lacked in some aspects due to resolution. It could also be that events present here are minor and not majorly significant. Otherwise, ice quality affected what could have been sampled and data was missed, which would have helped discern distinct events. There was not enough samples of Li^+ in which could have added to evidence of mineral dust and volcanic activity and Br^- values proved unreliable due to low signals that could not provide clear instances of variability and seasonality.

6.7 Conductivity, dust and drill liquid contamination

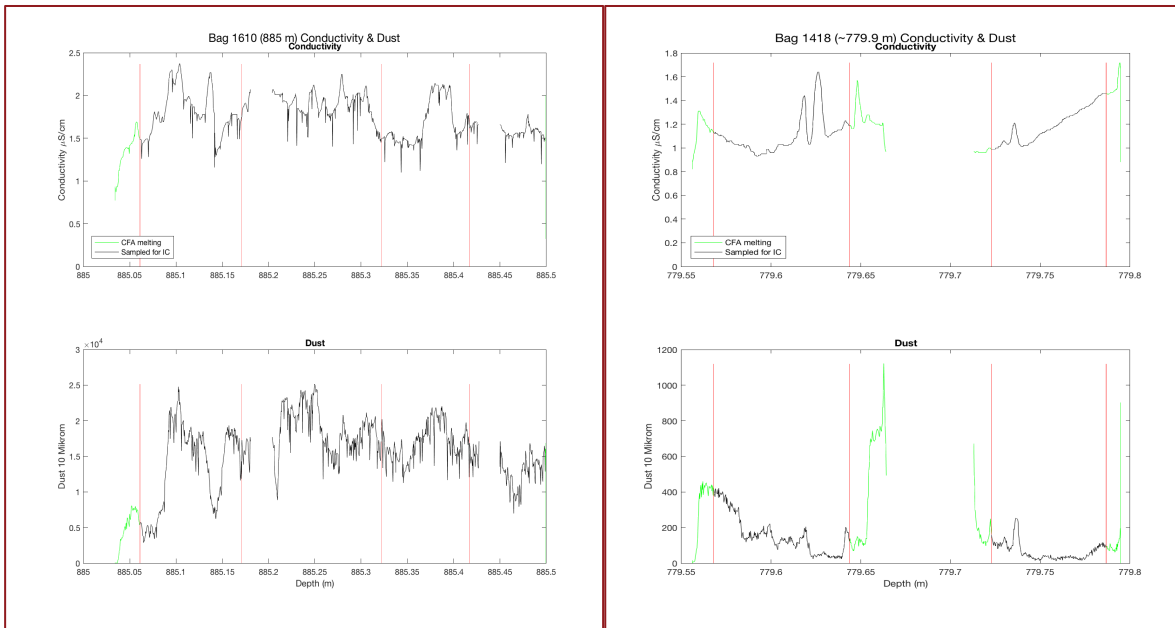


Figure 34 Conductivity and dust sampling from CFA with relatively more contamination from drill liquid (left) and less contamination (right). IC sampling (black) stopped where there was a break to reduce contamination (right).

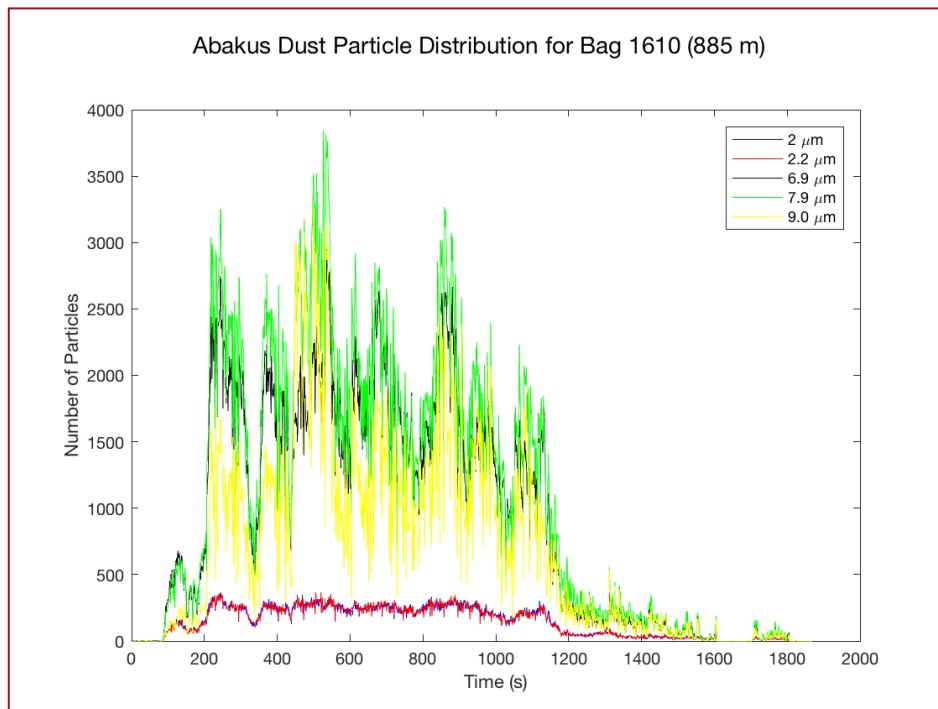


Figure 35 Abakus data for 885 m showing particle size distribution and the sizes in which most dust particles lie.

Figure 34 is shown as examples of conductivity and dust data from CFA melting of BZ samples. Figure 34 (right) shows how the procedure implemented in this study aimed to reduce contamination of samples by sampling where contamination was least likely to occur, as

indicated by black lines. This graph further shows that contamination was most frequent at the breaks. Dust values indicative of true signals from the ice are seen in Figure 34 (right).

In Figure 34 (left), dust data peaks at 2.5×10^5 particles, which is disproportionately higher than what is observed in true ice core dust signals. This is likely due to the presence of drill liquid. During the melting of the section of ice with drill liquid, there is no clear true signal of ice without contamination. Despite the areas of ice without a break, contamination is unable to wash out of CFA lines and the original baseline unable to be established. The high values observed in the dust sampling demonstrates that a period of time would be necessary after melting to wash out the lines of drill liquid to return to baseline as it would otherwise impact subsequent samples.

The dust particle distribution of ice with drill liquid contamination shows that many particles lie between 6.9 and 7.9 μm (Figure 35). If all or most contamination present in the ice is derived from drill liquid, then it would be feasible to say that drill liquid is present in ice cores as particles between 6.9 and 7.9 μm . Particles of 9.0 μm are also heavily present in the sample and largely following the same peaks as that of 6.9 and 7.9 μm particles, but are not observed at amounts of the same extent. In this sample, high amounts of Br⁻ were also detected and it is unclear where such contamination is derived from, drill liquid or otherwise (Figure 28). Analysis of exact ingredients of drill liquid used may help determine if the Br⁻ is derived from drill liquid contamination or another factor. If Br⁻ in this sample is derived from drill liquid then there is greater likelihood that contamination and particle size distribution shown above is representative of and limited to drill liquid and less so other sources of contamination. Further study into drill liquid contamination can take dust particle size measurements for several contaminated samples to determine and verify similar particle size distributions.

6.8 Limitations and Uncertainties

This project's limitations begin at the quality of ice itself that prevents classical CFA due to the many cracks and severed pieces that result in air bubbles and contamination in the CFA system. The effects would distort data upon sample entering the system and afterwards when contamination does not immediately wash out of the CFA lines, resulting in the use of the previously described method for sampling and analysis. However, there are still uncertainties.

The applied methodology integrated CFA to melt and decontaminate samples. Samples chosen were on an irregular basis due to ice quality and time constraint. In beginning and end of the BZ, there were more samples that fit the criteria for potential sampling, more than what the time constraint allowed for. However, in the middle of the BZ, ice quality further decreased, reducing the amount and choices in ice that fit the criteria for melting. The selection bias impacted the data that would be produced and analyzed. Events of interest, such as volcanoes forest fires could have been missed due to non-continuous sampling and selection of ice. The data are then a fragment of the entire timespan corresponding BZ and Holocene.

Irregularities, such as ice getting caught in the frame and broken corners on ice, caused interruptions in melting in which the encoder data was affected when air got into the system. The encoder data, representative of the meltrate at any given time of melting was later used to calculate relative depth. In turn, the relative depth calculation could have been affected despite the smoothing effects and constraints placed on the encoder data to minimize this.

Not all minor cracks were immediately visible and realized upon sampling and logging. With fragmented pieces that had no cracks, contamination was expected at the exposed top and bottom. Despite efforts to shave off contaminated areas, they still appeared to have entered the system at melting due to extremely irregular dust peaks.

The discrete nature of IC sampling creates results that are averaged over increments. Here, the increments vary between 5 cm of ice to about 10 cm in a vial, which dilutes signals of events of interest that would have otherwise been more visibly pronounced through CFA. This adds to the challenge of data analysis when some ions show relatively higher concentration values but others ions that are indicative of the same climate parameter show 'normal' values, leading to the uncertain conclusion whether a specific event occurred.

In data processing, there were uncertainties in calculating depth and adding breaks, as these calculations were based on the encoder that was, at times, affected by unstable melting, and also measurements based on the human eye and made in the cold room. Data interpolation was necessary in order to get the age with respect to concentrations, which may cause uncertainties if there were points with no exact matching value available for perfect interpolation.

7. Conclusion

This study integrated the use of CFA and IEC on the IC to study the NEEM BZ, as traditional CFA methods have not been applied previously due to poor ice quality. While there are limitations and uncertainties, data points were produced for the Holocene period between ~3900 and 7200 years B2K. The data were compared with published data in order to determine the extent and likeliness in which true values were produced (and where signals could not be discerned). Particular events were pointed out and investigated further in which reasoned hypothesis were provided to conclude that particular climate events or intense seasons may have occurred. A broad study on drill liquid contamination in brittle ice yielded information about particle size and effects in conductivity, dust and chemistry data.

The results showed that the chemistry data is comparable with that of published data. Means and standard deviations were provided to demonstrate variability. Bromine data differed but possible reasons were provided. Based on these comparisons, it is evident that NEEM brittle data has been absent until now. In each study case at various depths, hypotheses were supported by evidence where available and otherwise deemed inconclusive. More samples are needed and further work could include the continuation of the method outlined in this study to produce more datapoints. This may alter the average values produced in this study and may make them more comparable to published data and decrease overall data fragmentation. Drill liquid contamination also posed an interesting study about contamination, dust and particle sizes. Based on this study, Holocene climate was, as expected, reasonably stable but variability creates interesting instances for chemistry study.

References

- Baroni, M. et al., 2008. Anomalous sulfur isotope compositions of volcanic sulfate over the last millenium in Antarctic ice cores. *Journal of Geophysical Research*, Volume 113, pp. 1-12.
- Bigler, M. et al., 2011. Optimization of High-Resolution Continuous Flow Analysis for Transient Climate Signals in Ice Cores. *Environmental Science and Technology*, Volume 45, pp. 4483-4489.
- Cole-Dai, J. et al., 2009. Cold decade (AD 1810-1819) caused by Tambora (1815) and another (1809) stratospheric volcanic eruption. *Geophysical Research Letter*, Volume 36.
- Dixon, D. et al., 2011. An ice-core proxy for northerly air mass incursions into West Antarctica. *International Journal of Climatology*, Volume 32, pp. 1455-1465.
- Fischer, H. et al., 2015. Millennial changes in North American wildfire and soil activity over the last glacial cycle. *Nature Geoscience*, Volume 8, pp. 723-727.
- Fischer, H. et al., 2007. Glacial/interglacial changes in mineral dust and sea salt records in polar ice cores: Sources, transport and deposition.. *Review of Geophysics*, 45(1).
- Gabrielli, P. et al., 2005. Variations in atmospheric trace elements in Dome C (East Antarctica) ice over the last two climate cycles. *Atmospheric Environment*, 39(34), pp. 6420-6429.
- Kaufmann, P. et al., 2008. An Improved Continuous Flow Analysis System for High-Resolution Field Measurements on Ice Cores. *Environmental Science and Technology*, Volume 42, pp. 8044-8050.
- Kipfstuhl, S., Pauer, F., Kuhs, W. F. & Shoji, H., 2001. Air bubbles and clathrate hydrates in the transition zone of the NGRIP deep ice core. *Geophysical Research Letters*, 28(4), pp. 591-594.
- Kopaciewicz, W., Rounds, M. A., Fausnaugh, J. & Regnier, F. E., 1983. Retention model for high-performance ion-exchange chromatography. *Journal of Chromatography*, Volume 266.

Laluraj, C. M. et al., 2010. Nitrate records of a shallow ice core from East Antarctica: Atmospheric processes, preservation and climatic implications. *The Holocene*, 21(2).

Lambert, F. et al., 2008. Dust-climate couplings over the past 800,000 years from the EPICA Dome C ice core.. *Nature*, Volume 452, pp. 616-619.

Legrand, M. & Mayewski, P., 1997. Glaciochemistry of Polar Ice Cores: A Review. *Review of Geophysics*, 35(3), pp. 219-243.

Neff, P., 2014. A review of brittle ice zone in polar ice cores. *Annals of Glaciology*, 55(68), pp. 72-82.

Popp, T. J., Hansen, S. B., Sheldon, S. G. & Panton, C., 2014. Deep ice-core drilling performance and experience at NEEM, Greenland. *Annals of Glaciology*, 55(68), pp. 53-64.

Röthlisberger, R. et al., 2000. Technique for Continuous High-Resolution Analysis of Trace Substances in Firn and Ice Cores. *Environmental Science and Technology*, Volume 34, pp. 338-342.

Röthlisberger, R. et al., 2002. Nitrate in Greenland and Antarctic ice cores: a detailed description of post-depositional processes. *Annals of Glaciology*, Volume 35, pp. 209-216.

Rasmussen, S. O. et al., 2013. A first chronology for the North Greenland Eemian Ice Drilling (NEEM) ice core. *Climate of the Past*, Volume 9, pp. 2713-2730.

Schüpbach, S. et al., 2018. Greenland records of aerosol source and atmospheric lifetime changes from the Eemian to the Holocene. *Nature Communications*, Volume 9.

Sheldon, S. G. et al., 2014. The investigation and experience of using Estisol 240 and Coasol for ice drilling. *Annals of Glaciology*, 55(68), pp. 219-232.

Sigg, A. et al., 1994. A Continuous Analysis Technique for Trace Species in Ice Cores. *Environmental Science and Technology*, Volume 34, pp. 338-342.

Siggard-Andersen, M., Steffensen, J. P. & Fischer, H., 2002. Lithium in Greenland ice cores measured by ion chromatography. *Annals of Glaciology*, Volume 35, pp. 243-249.

Simonsen, M. F. et al., 2018. Particle shape accounts for instrumental discrepancy in ice core dust size distribution. *Climate of the Past*, 14(5), pp. 601-608.

Soon, W. et al., 2014. A review of Holocene solar-linked climatic variation on centennial to millennial timescales: Physical processes, interpretative frameworks and a new multiple cross-wavelet transform algorithm. *Earth-Science Reviews*, Volume 134.

Spolaor, A. et al., 2016. Canadian Arctic sea ice reconstructed from bromine in the Greenland NEEM ice core. *Scientific Reports*, 6(33925).

Svensson, A., 2014. Ice Cores. *Encyclopedia of Scientific Dating Methods*.

Svensson, A., Biscaye, P. & Grousset, F., 2000. Characterization of late glacial continental dust in Greenland Ice Core Project ice core. *Journal of Geophysical Research*, 105(D4), pp. 4637-4656.

Talalay, P., 2011. *Technical Report: PRC 12-01 Drilling Fluids for Deep Coring in Central Antarctica*, Jilin University, China: Polar Research Center.

Taylor, K. C. et al., 1993. Electrical conductivity measurements from the GISP2 and GRIP Greenland ice cores. *Nature*, Volume 366, pp. 549-552.

Uchida, T. et al., 1994. Brittle zone and air-hydrate formation in polar ice sheets. *Memoirs of National Institute of Polar Research*, Issue 49, pp. 298-305.

Vallelonga, P., Barbante, C., Cozzi, G. & Gaspari, V., 2004. Elemental indicators of natural and anthropogenic aerosol impurities at Law Dome, Antarctica. *Annals of Glaciology*, Volume 39, pp. 169-174.

Wilhelms, F. et al., 1998. Precise dielectric profiling of ice cores: a new device with improved guarding and its theory. *Journal of Glaciology*, Volume 44, pp. 171-174.

Appendix

Appendix A: Calculation of nSs component of sea salt ions.

Table 1. General constituents of seawater

Seawater Ionic Species	Constituent (g/kg) in 34.7 PSU seawater
Chloride (Cl ⁻)	19.162
Sodium (Na ⁺)	10.679
Magnesium (Mg ²⁺)	1.278
Calcium (Ca ²⁺)	0.4096
Potassium (K ⁺)	0.3953

Source: Britannica

Calculation of Sea Salt Ratios

Formula:

$$\text{Non-sea salt Na}^+ = \text{nSs Na}^+ = [\text{Na}^+_{\text{measured}}] - (\text{Na}^+_{\text{seawater}}/\text{Cl}^-_{\text{seawater}})*[\text{Cl}^-_{\text{measured}}]$$

$$\text{Cl}^-_{\text{seawater}} = 19.162 \text{ g/kg} = 1.1916*10^7 \text{ ppb}$$

$$\text{Na}^+_{\text{seawater}} = 10.679 \text{ g/kg} = 1.068*10^7 \text{ ppb}$$

$$\text{Average IC Na}^+ = 7.3529 \text{ ppb}$$

$$\text{Average IC Cl}^- = 18.4847 \text{ ppb}$$

$$\text{nSs Na}^+ = 7.3529 - (1.068*10^7 / 1.1916*10^7)* 18.4847$$

$$\text{nSs Na}^+ = -2.9507$$

This calculation was applied for Cl⁻, Mg²⁺, Ca²⁺, and K⁺ using the above assumed ratios of ions in seawater.

